STEM CELLS

DOT1L is a barrier to histone acetylation during reprogramming to pluripotency

Coral K. Wille[1]†, Xiaoya Zhang[1,2]†, Spencer A. Haws[1,3], John M. Denu[1,3], Rupa Sridharan[1,4]*

Embryonic stem cells (ESCs) have transcriptionally permissive chromatin enriched for gene activation–associated histone modifications. A striking exception is DOT1L-mediated H3K79 dimethylation (H3K79me2) that is considered a positive regulator of transcription. We find that ESCs are depleted for H3K79me2 at shared locations of enrichment with somatic cells, which are highly and ubiquitously expressed housekeeping genes, and have lower RNA polymerase II (RNAPII) at the transcription start site (TSS) despite greater nascent transcription. Inhibiting DOT1L increases the efficiency of reprogramming of somatic to induced pluripotent stem cells, enables an ESC-like RNAPII pattern at the TSS, and functionally compensates for enforced RNAPII pausing. DOT1L inhibition increases H3K27 methylation and RNAPII elongation–enhancing histone acetylation without changing the expression of the causal histone-modifying enzymes. Only the maintenance of elevated histone acetylation is essential for enhanced reprogramming and occurs at loci that are depleted for H3K79me2. Thus, DOT1L inhibition promotes the hyperacetylation and hypertranscription pluripotent properties.

INTRODUCTION

During development, master transcription factors are necessary for lineage commitment because they control cell type–specific gene expression (*1*, *2*). The introduction of such master regulators can even change the identity of already specified terminally differentiated cells (*3*). For example, the transcription factors OCT4 (POU5F1), SOX2, KLF4, and c-MYC are sufficient to reprogram somatic cells to induced pluripotent stem cells (iPSCs) (*4*). Both lineage commitment and cell identity conversion are facilitated by a conducive epigenetic landscape (*5*–*7*). Histone posttranslational modifications (PTMs) are a primary determinant of the epigenetic environment and act through several broad mechanisms. These include directly affecting chromatin compaction by changing nucleosome surface charge and influencing the recruitment of chromatin remodeling enzymes to permit master regulator binding for RNA polymerase II (RNAPII)–mediated transcription.

In contrast to unipotent differentiated cells, pluripotent stem cells such as embryonic stem cells (ESCs) maintain their own identity while remaining poised for differentiation. These pluripotent properties are enabled by a less compacted chromatin structure (*8*) whose features can be measured quantitatively by mass spectrometry for histone PTM abundance. ESCs are depleted for histone PTMs associated with gene repression and enriched for those associated with gene activation, such as acetylation (*9*). The open chromatin structure also allows ESCs to have a greater mRNA output per cell than somatic cells (*10*, *11*), a phenomenon called hypertranscription (*12*).

Paradoxical to this notion of a transcription-ready chromatin structure, ESCs are severely depleted for histone H3K79 methylation (me) (*9*). H3K79me is assumed to be a positive regulator of transcription because it is enriched on the gene bodies of highly and rapidly transcribed genes in somatic or transformed cell lines (*13*–*15*). While histone modifications at promoters and enhancers reinforce cell-specific transcriptional programs, whether gene body modifications, such as H3K79me2, are causal to cell identity is unexplored. DOT1L (disrupter of telomeric silencing 1-like) is the only enzyme that deposits H3K79 mono-, di-, and trimethylation (*16*). H3K79 methylation is thought to be removed by nucleosome turnover (*17*, *18*). Despite their hypertranscriptional state, ESCs actively translocate DOT1L to the cytoplasm to maintain low nuclear levels (*19*).

While knockout (KO) *Dot1l* ESCs continue to self-renew (*20*, *21*), DOT1L pharmacological inhibition enhances generation of totipotent 2 cell-like cells (2CLC) (*22*) via chromatin reorganization (*23*). By contrast, loss of DOT1L activity impairs differentiation of ESCs in vitro (*21*, *24*) and KO-*Dot1l* mice die around embryonic day 11.5 (*20*, *25*, *26*). Catalytic inhibition or depletion of DOT1L greatly increases cellular reprogramming efficiency from somatic to iPSCs (*27*, *28*). Hence, low levels of DOT1L activity are conducive to and even enhance pluripotency, but H3K79me is necessary for establishing somatic identity (*29*). Contradictory to the proposed role of H3K79 methylation as a positive regulator of transcription, compromising DOT1L leads to few steady-state transcriptional changes in ESCs (*21*, *24*) or during reprogramming, where we have found that no single altered gene is able to replace DOT1L inhibitor effects (*28*). DOT1L must even be excluded from the nucleus when the zygotic genome is activated for transcription at the two-cell stage (*23*) for continued growth (*30*). Together, the functional role of H3K79 methylation is likely to be wide-ranging, yet how DOT1L profoundly affects cell fate change remains unknown.

Here, we find that in ESCs, H3K79 methylation is lowered at genes that are also modified in somatic cells. Depletion of H3K79me2 is concomitant with an increase in elongating RNAPII in pluripotency. During the reprogramming of somatic cells to iPSCs, lowering H3K79 methylation by DOT1L inhibition functionally counteracts the negative effects of enforced RNAPII pausing. In response to DOT1L inhibition, we find an increase in

[1]Wisconsin Institute for Discovery, University of Wisconsin-Madison, Madison, WI 53715, USA. [2]Laboratory of Genetics, University of Wisconsin-Madison, Madison, WI 53706, USA. [3]Department of Biomolecular Chemistry, University of Wisconsin-Madison, Madison, WI 53706, USA. [4]Department of Cell and Regenerative Biology, University of Wisconsin-Madison, Madison, WI 53705, USA.
*Corresponding author. Email: rsridharan2@wisc.edu
†These authors contributed equally to this work.

histone acetylation in both ESCs and reprogramming populations by quantitative mass spectrometry. Early in reprogramming, before the appearance of iPSC colonies, this histone acetylation is elevated at ubiquitously expressed genes, rather than lineage-specific genes. Maintaining higher histone acetylation enhances reprogramming efficiency. Conversely, increasing DOT1L in ESCs decreases transcription. DOT1L thus emerges with important roles in balancing histone acetylation and hypertranscription, two key properties of pluripotency to enable cell fate change.

RESULTS

ESCs have lower H3K79me2 enrichment than somatic cells at shared genic locations

We were intrigued by the preference of pluripotent stem cells for low H3K79 methylation levels (*20*, *21*, *23*, *24*). H3K79me2 was the most differential histone PTM between ESCs and mouse embryonic fibroblasts (MEFs) measured by quantitative mass spectrometry (*9*). H3K79me2 levels in ESCs are also three- to fivefold lower in other somatic cells such as keratinocytes (*28*) and astrocytes (fig. S1A). This difference in H3K79 methylation levels was not due to the faster cell cycle of ESCs, since cell cycle–arrested ESCs did not accumulate MEF levels of H3K79me2 (fig. S1B). To gain insight into the genomic distribution of H3K79me2, we performed quantitative chromatin immunoprecipitation sequencing (ChIP-seq) with a spike in control (*31*). In both MEFs and ESCs, 95% of H3K79me2 peaks are enriched on gene bodies (fig. S1C). As expected, MEF- and ESC-specific genes had a greater enrichment of H3K79me2 in the respective cell types (Fig. 1, A to E, and fig. S1D). Surprisingly, 80% of H3K79me2-enriched genes overlap in both cell types (Fig. 1A), suggesting that the increased levels of this modification in MEFs do not occur at unique locations. Instead, ESCs have a lower enrichment of H3K79me2 at shared genes (Fig. 1, B and C).

DOT1L is a distributive enzyme, and the degree of H3K79 methylation depends on its local abundance (*32*). We wondered whether H3K79 mono- or trimethylation, whose functions are not well studied, might be elevated in the place of H3K79me2 at shared genes in ESCs (fig. S1, E and F). Like H3K79me2, ChIP-seq for H3K79me3 revealed a sharp peak at the transcription start site (TSS) of genes (Fig. 1E) in both ESCs and MEFs with ~3-fold greater enrichment in MEFs (Fig. 1F). In contrast to H3K79me2/me3, H3K79me1 showed a TSS enrichment in ESCs and was evenly distributed across the gene body in MEFs (Fig. 1, E and F). Therefore, the different degrees of H3K79 methylation have a cell type–specific distribution pattern in pluripotent and somatic cells.

ESCs are enriched for H3K79me1 instead of H3K79me2/me3 at highly expressed essential genes

We noticed that genes with shared H3K79me2 enrichment in both cell types were much more highly expressed than either MEF or ESC lineage-specific genes (Fig. 1D). To further investigate how gene expression was influenced by the level of H3K79 methylation modification in each cell type, we binned genes into four groups based on steady-state RNA-sequencing (RNA-seq) measurements: high [>40 transcripts per million (TPM)], middle (12 to 40 TPM), low (2 to 12 TPM), or off (<2 TPM). Genes with shared H3K79me2 enrichment between ESCs and MEFs were expressed in both cell types (fig. S2A), and most (~70%) remained within the same expression bin (Fig. 1G). In both MEFs and ESCs, higher expression correlated with total H3K79 methylation (me1 + me2 + me3) (fig. S2B). However, ESCs had significantly more H3K79me1 and less H3K79me2/3 at highly expressed genes as compared to MEFs (Fig. 1, H and I, and fig. S2, C to E). Given their common high expression, we examined gene expression data in several terminally differentiated cell types from distinct lineages such as keratinocytes, immune-related B cells, and brain cells from the telencephalon and found that the shared H3K79me2 genes were always highly expressed (Fig. 1J). Enrichment of H3K79me1 is a better indicator of gene expression in ESCs as compared to H3K79me2/3 in MEFs, even at highly and ubiquitously expressed genes. Furthermore, ESCs can maintain high steady-state expression without H3K79me2/me3.

ESCs have greater RNAPII elongation as compared to somatic cells

ESCs actively translocate DOT1L to the cytoplasm (*19*), which likely prevents higher-order H3K79me. Therefore, we investigated if low DOT1L and H3K79me2/3 are features or facilitators of pluripotency. Steady-state gene expression levels are dependent on the rates of transcription, mRNA processing, and degradation (*33*). Transcription rate itself is determined by RNAPII initiation, release of RNAPII from pausing at about 50 base pairs (bp) downstream of the TSS, and elongation through the gene body (*34*–*38*). Since H3K79 methylation occurs on genes after transcription is initiated (*39*), we interrogated the relationship between cell type–specific levels of H3K79 methylation and RNAPII dynamics. We performed quantitative ChIP-seq for RNAPII in ESCs and MEFs, and interrogated the relative enrichment at the TSS compared to the gene body to determine the RNAPII traveling ratio (TR) (*40*). ESCs display a significantly lower TR compared to MEFs at genes with shared H3K79me2 enrichment (Fig. 2A, list from Fig. 1A) even at genes that were in the high expression bin and ubiquitously expressed in many cell types (keratinocytes, brain, and B cells) (fig. S3A). ESCs have much greater protein levels of RNAPII (Fig. 2B) and the general transcription factor TFIID (*41*) that promotes RNAPII initiation. Yet, unexpectedly, ESCs have a lower TR than MEFs because of less RNAPII enrichment at the TSS than the gene body (Fig. 2A). We confirmed these genome-wide results with ChIP-qPCR (quantitative polymerase chain reaction) at three candidate genes with widely differing TRs in ESCs and MEFs (fig. S3B and Fig. 2E).

We then asked how H3K79 methylation correlated with TR. The enrichment of H3K79me1/2/3 at the pause site was better correlated with TR at all genes compared to other characteristics such as expression level, gene length, and the number of introns (fig. S3C). At genes with a shared H3K79me2 peak in both ESCs and MEFs, isolated for the highest (Q1) or lowest (Q4) TRs, TR correlated with H3K79me3, H3K79me2, and gene length in both MEFs and ESCs (fig. S3C). In highly expressed genes with similar steady-state expression in both ESCs and MEFs, a low TR corresponded with low H3K79me2/me3 at the TSS (Fig. 2C). In ESCs, genes with a lower TR had a post-TSS shifted pattern of H3K79me1 and H3K79me2 (Fig. 2C), which could reflect a faster moving RNAPII that carries DOT1L along with it. Depending on in vitro culture conditions, mouse ESCs can exist in a continuum of pluripotent states that resemble the early blastocyst (serum-free 2i/LIF) or late blastocyst (serum/LIF). A transitional formative state that is germ

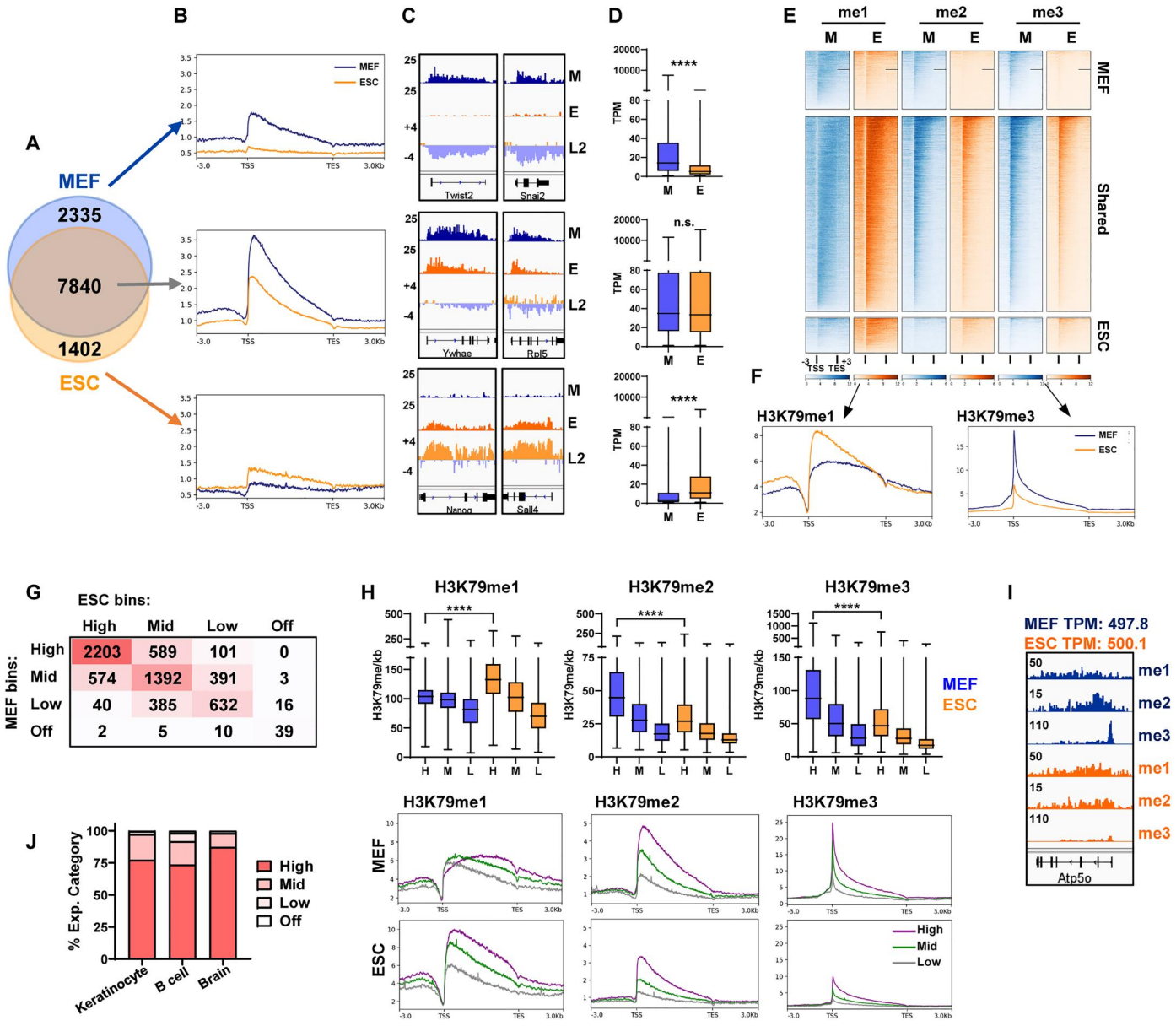

Fig. 1. ESCs have lower H3K79me2 enrichment than somatic cells at shared genic locations. (**A**) Overlap of genes with H3K79me2 peaks in MEFs (blue) and ESCs (orange). (**B** to **E**) Genes with H3K79me2 peaks in MEF (M) unique, ESC (E) unique, and shared were assessed for (B) relative H3K79me2 levels as metaplots. (C) Example H3K79me2 IGV tracks (L2 = $\log_2$ fold change ESC/MEF). (D) Expression (TPM). ****$P < 0.0001$ and not significant (n.s.) $P > 0.05$ by unpaired two-tailed t test. (E) H3K79me1, H3K79me2, and H3K79me3 enrichment. (**F**) Metaplot of H3K79me1 and H3K79me3 at shared genes with H3K79me2 peaks. (**G**) Comparison of expression category of genes with shared H3K79me2 peaks in ESCs versus MEFs. (**H**) Top: Normalized H3K79me genebody reads per kb gene length at high (H), middle (M), and low (L) expressed genes with shared peaks. ****$P < 0.0001$ by one-way ANOVA with the Tukey-Kramer post hoc test to make pairwise comparisons. Bottom: Metaplots of H3K79me1/2/3 at high (purple), middle (green), and low (gray) expressed genes with shared H3K79me2 peaks. (**I**) H3K79me1/2/3 IGV tracks at a gene with shared H3K79me2 peaks and similar steady-state expression. (**J**) Percent of MEF/ESC high [(G); $n = 2203$] per expression category in other cell types: keratinocytes (*84*), immature splenic B cell (*65*), and brain telencephalon (*85*).

cell competent can also be captured (*42*). It was recently reported that RNAPII elongates slower in 2i/LIF conditions (*43*). We passaged serum/LIF ESCs, in which all the preceding experiments were performed, into either 2i/LIF or formative conditions (fig. S3D). The serum/LIF ESCs had less H3K79me2 than 2i/LIF ESCs (Fig. 2D). Formative state ESCs had even lower levels of H3K79me2 than serum/LIF ESCs perhaps reflective of a faster RNAPII elongation rate. Together, these results suggest that there is an inverse correlation between RNAPII rate and H3K79 methylation accumulation in the pluripotency continuum.

The decreased TSS-associated RNAPII as well as the gene body shifted H3K79 methylation signal suggests that in ESCs, RNAPII may transition from pause to elongation more efficiently than MEFs. To directly measure the transition to elongation, RNAPII

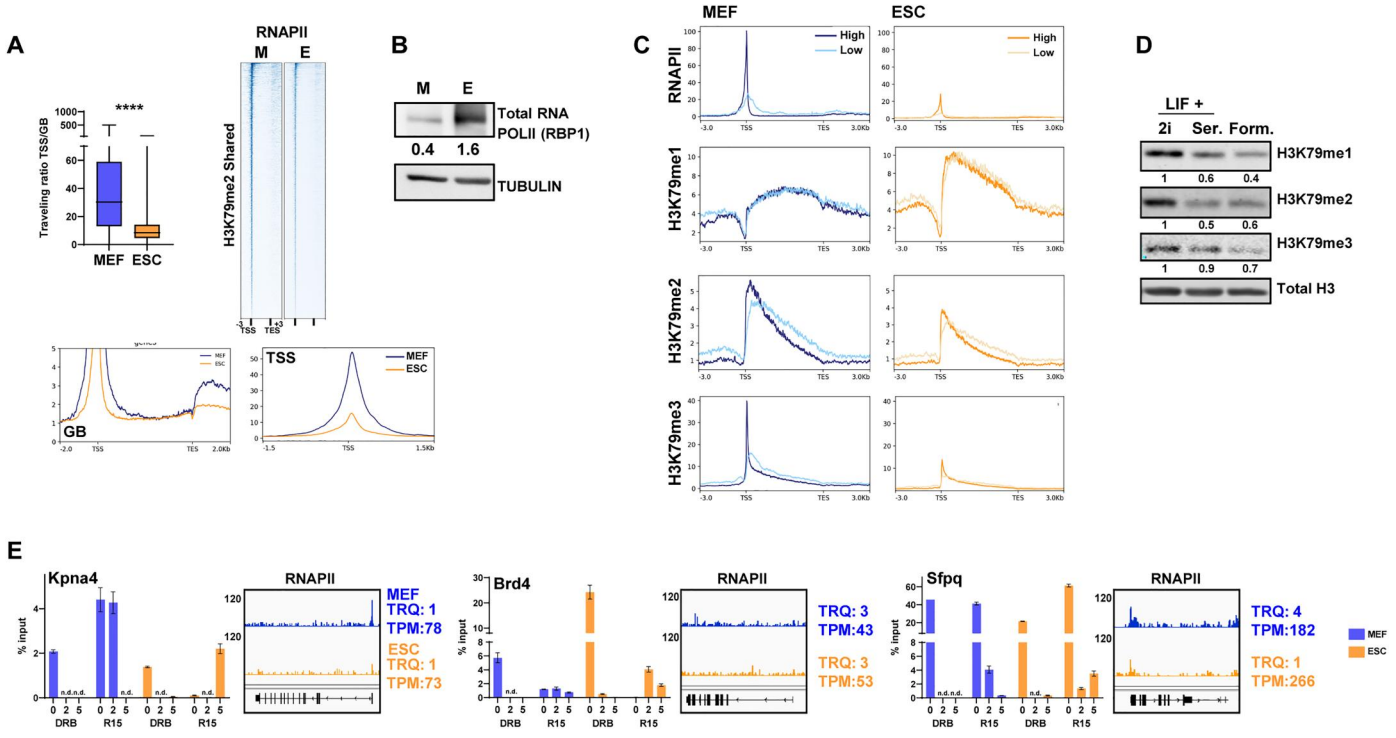

Fig. 2. ESCs have greater RNAPII elongation compared to somatic cells. (**A**) RNAPII analysis at H3K79me2-shared genes (Fig. 1A) in MEFs (M) and ESCs (E) of TR (top left). Data are the mean ($n = 2$). ****$P < 0.0001$ by unpaired two-tailed t test. Bottom: RNAPII metaplots centered at the TSS or genebody (GB). Top right: RNAPII heatmap. (**B**) RNAPII immunoblot in MEFs (M) and ESCs (E). (**C**) RNAPII and H3K79me1/2/3 metaplots at H3K79me2-shared genes, with high and similar expression (within twofold TPM in MEFs and ESCs) of the highest (dark) and lowest (light) quartile of traveling ratio ($n = 415$ genes per quartile). (**D**) H3K79me immunoblot of pluripotent cells in LIF + 2i, LIF + Serum (Ser.), and Formative (Form.) conditions. (**E**) RNAPII ChIP-qPCR of MEFs (blue) and ESCs (orange) treated for 3 hours with DRB and, 15 min after release (R15) from DRB pause, at specified distances from TSS. Inset: Expression (TPM) and TR quartile (TRQ) in MEFs (blue) and ESCs (orange).

was paused with the addition of 5,6-dichloro-1-β-D-ribofuranosylbenzimidazole (DRB) and then released for 15 min. We then performed ChIP-qPCR for three candidate genes with varying TR in ESC and MEFs at the pause site (0 kb) and 2 and 5 kb within the gene body. In all three cases, there was more enrichment of RNAPII in the gene body in ESCs than in MEFs, indicating a faster RNAPII elongation rate, or potentially a faster reinitiation given the abundance of RNAPII in ESCs (Fig. 2E).

Increasing DOT1L levels in ESCs can reduce nascent transcription

We measured if there was a difference in nascent RNA output that reflected the differential RNAPII elongation pattern in MEFs and ESCs (Fig. 2). Upon DRB-mediated pause release, we captured de novo synthesized RNA by incubating cells in the presence of 5-ethynyl uridine (EU) for 30 min. To gain a gene-centric view of nascent RNA production, we chose three candidate RNAPII transcribed loci that perform essential functions in widely different pathways—chromatin remodeling (Brd4), splicing (Sfpq), and intracellular secretion (Sppl3)—which were highly and evenly expressed in MEFs and ESCs by steady-state measurements (Fig. 3A). After pausing RNAPII with DRB, we measured EU-labeled nascent RNA by reverse transcription qPCR (RT-qPCR). At locations ranging from 0.5 to 2 kb or more from the TSS, we found that ESCs had a greater amount of nascent RNA at all three loci than MEFs (Fig. 3A and fig. S4A). Moreover, ESCs had more nascent RNA in the presence of DRB even before release, indicating a lower uptake or sensitivity to DRB and/or pause regulation (Fig. 3A and fig. S4A) in accordance with lower relative RNAPII occupancy at the TSS in ESCs (Fig. 2A).

To gain a global view of nascent RNA production in single cells, we measured newly synthesized (nascent) RNA in single cells by coupling EU incorporation to a fluorescent readout (Fig. 3B). Using flow cytometry, ESCs had significantly more nascent RNA (~4-fold compared to DRB control) after DRB release as compared to MEFs (~2-fold compared to DRB control) (Fig. 3C and fig. S4B). This difference in nascent RNA was consistently observed even after inhibiting RNAPI (Fig. 3B and fig. S4C).

To directly test the causal connection between de novo RNA synthesis and H3K79 methylation, we subjected ESCs and MEFs to a small-molecule pharmacological inhibitor of DOT1L catalytic activity, SGC0946 (DOT1Li) (*44*), for 2 days. This inhibitor lowers DOT1L association with chromatin and thus may also function by reducing local enzyme concentration (*45*). Globally, under DRB-pause release conditions, there was no significant difference in EU-labeled RNA in either cell type by flow cytometry (fig. S4D). Similarly, at the locus-specific level, we did not find a consistent trend in nascent RNA production in MEFs and ESCs (Fig. 3D and fig. S4E) at exemplar genes (criteria in fig. S4E). Under non-paused conditions, there was a small but statistically nonsignificant decrease in EU-labeled RNA in MEFs, but not in ESCs (fig. S4D). Thus, lowering H3K79me2 in MEFs and ESCs with DOT1Li

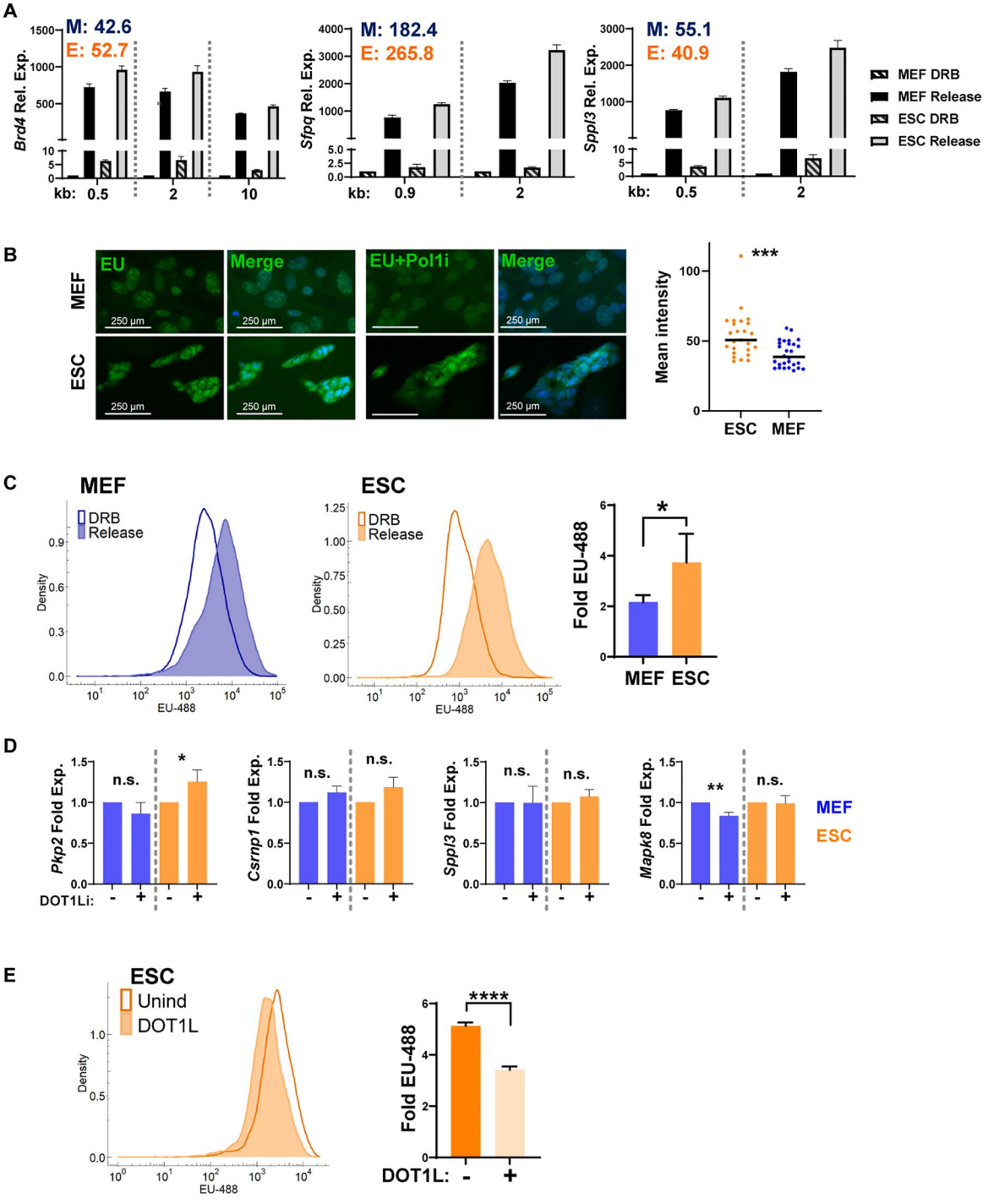

Fig. 3. Increasing DOT1L levels in ESCs can reduce nascent transcription. (**A** to **C**) Nascent RNA EU profiling in MEFs and ESCs. Transcription was halted with DRB. A control sample (DRB) was collected, and then transcription was released for 30 min in the presence of EU. (A) EU-containing RNA was enriched and then measured by RT-qPCR. Unreleased DRB MEFs set to 1. Inset: MEF (M) and ESC (E) steady-state expression (TPM). (B) Cells were treated with the RNA polymerase I inhibitor (Pol1i) CX-5461 (fig. S4C) or not. EU was labeled with a 488-fluorophore and imaged with microscopy. Right: EU-488 signal of cells released in the presence of Pol1i was quantitated and plotted as mean nuclear intensity (n = 30 nuclei). ***$P < 0.001$ by unpaired two-tailed t test. (C) EU was labeled with a 488-fluorophore, and signal/cell was measured by flow cytometry. Left: EU-488 signal density plot. Outline = DRB unreleased; shaded = released in EU. Right: Fold increase of EU-488 signal after release, DRB sample set to 1. Data are the mean + SD (n = 3). *$P < 0.05$ by ratio paired two-tailed t test. (**D**) Nascent RNA intron profiling in MEFs and ESCs treated with DOT1Li (+) or control (–). After DRB pause, transcription was released for 15 min and nascent RNA was measured with intron RT-qPCR. Released, control treated cells set to 1. Data are the mean + SD (n = 3). **$P < 0.01$, *$P < 0.05$, and not significant (n.s.) $P > 0.05$ by unpaired two-tailed t test. (**E**) Nascent RNA EU profiling in ESCs with and without DOT1L-induced expression. Left: Flow cytometry EU-488 signal density plot. Outline = uninduced (Unind) control ESCs; shaded = ESCs induced to express DOT1L for 3 days. Right: Fold increase of EU-488 signal after release, DRB sample set to 1. Data are the mean + SD (n = 3). ****$P < 0.0001$ by unpaired two-tailed t test.

treatment likely results in locus-specific, but not global, alternations in transcription.

Rather than decrease H3K79 methylation levels with DOT1L inhibition, we performed the reciprocal experiment of increasing DOT1L levels. We integrated full-length DOT1L into a single locus in the genome that was controlled by a doxycycline-inducible promoter in ESCs. Doxycycline induction increased DOT1L levels by 17-fold, with a concomitant increase in H3K79me1 by 1.7-fold, H3K79me2 by 4.9-fold, and H3K79me3 by 2.5-fold (fig. S4F). After DRB-pause release, there was a ~2-fold reduction in newly synthesized RNA in the DOT1L-induced ESCs when compared to uninduced control (Fig. 3E), but not in the doxycycline-induced ESCs that do not overexpress the transgene (fig. S4G). These data further cement cell type–specific relationships between H3K79 methylation and transcriptional elongation. Nascent transcription in ESCs is agnostic to further lowering of DOT1L activity but sensitive to increased DOT1L levels. In MEFs, the removal of H3K79 methylation is insufficient to cause an ESC-like hypertranscriptional state. Therefore, to further understand the connection between H3K79 methylation and cell fate, we turned to the dynamic system of somatic cell reprogramming.

Erasure of H3K79 methylation promotes reprogramming by altering RNAPII dynamics

While DOT1L is dispensable for the maintenance of ESCs (*20*, *21*, *24*), its catalytic activity is a barrier to the reprogramming of mouse and human somatic cells to iPSCs (*27*, *28*, *46*). Our previous results have shown that DOT1L inhibition does not increase reprogramming efficiency by affecting lineage-specific gene expression (*28*). Therefore, we investigated whether reducing H3K79 methylation causally influenced this change in cell identity by altering RNAPII dynamics.

We induced reprogramming in MEFs that have a single transgenic copy of *Oct4*, *Sox2*, *c-Myc*, and *Klf4* (OSKM) integrated into the genome under a doxycycline promoter in conjunction with DOT1Li. Upon DOT1Li, we observe a ~15-fold increase in colonies expressing the pluripotency factor NANOG in the presence of OSKM transgene expression by day 6 (Fig. 4A and fig. S5A). A stringent measure of bona fide iPSC formation is sustained pluripotency without exogenous OSKM transgene expression, which we measure by withdrawing doxycycline and DOT1Li (Fig. 4A). Although the total number of $NANOG^+$ colonies decreases after the OSKM transgene is turned off (fig. S5A), DOT1Li increases transgene-independent stable iPSCs by 30-fold (Fig. 4A).

Using this system, we interrogated the localization of H3K79me1/2/3 upon DOT1Li. We performed ChIP-seq on day 4 of reprogramming, even before the appearance of transgene-dependent $NANOG^+$ colonies (fig. S5B), to capture the molecular effects in the transition to pluripotency, albeit in a heterogeneous population. DOT1Li greatly reduced H3K79me1, H3K79me2, and H3K79me3 enrichment (Fig. 4B and fig. S5C). The remainder of the peaks after DOT1Li exposure were still genic and retained at genes with the highest expression (fig. S5, D and E).

We then performed ChIP-seq for RNAPII in reprogramming populations to determine transcriptional dynamics with reduced H3K79me. DOT1Li populations had lowered TR as compared to the control due to a decrease in RNAPII at the TSS (Fig. 4C), making the pattern of enrichment resemble that in ESCs (Fig. 2A). The gene body enrichment of RNAPII in DOT1Li-exposed cells was also lower than in control reprogramming populations (Fig. 4C). This is likely because the total RNAPII protein does not reach the levels observed in ESCs by day 4 of reprogramming (Fig. 4D). Thus, removal of H3K79me during reprogramming allows cells to acquire a more pluripotency-like RNAPII enrichment pattern.

To uncover the functional consequence of this lowered TR, we measured nascent RNA production. DOT1Li-treated reprogramming populations had a ~3.4-fold increase in total nascent transcripts as compared to ~2.6-fold in control treatment (Fig. 4E and fig. S5F) after DRB-pause release. Even in a heterogeneous reprogramming population with lower levels of RNAPII as compared to ESCs, DOT1Li leads to a greater accumulation of nascent RNA. We next tested whether this small increase in RNA synthesis facilitated pluripotency. While DRB is toxic at high concentrations, at lower concentrations, it can be used to pause RNAPII without excessive cell death (*47*). We performed reprogramming in the presence of nontoxic levels of DRB, which yielded a reduced number of iPSCs. Reprogramming efficiency was restored to control levels when DOT1Li was added in conjunction with DRB (Fig. 4F and fig. S5G). Despite the caveats of DRB having other off-target effects, these results support the idea that changing nascent RNA accumulation contributes to the cell fate change to pluripotency.

Low DOT1L activity enables higher histone acetylation

As we (*28*) and others (*21*, *24*, *27*) have found few DOT1L-mediated transcriptional effects on the regulation of single genes in pluripotency, we next interrogated if loss of H3K79me affects the epigenome on a large scale. While it is well established that transcriptional output is affected by histone modification, less is known about the histone code around RNAPII processivity. We used mass spectrometry to quantify global levels of histone PTMs in an unbiased way (fig. S6, A and B) in MEFs and ESCs subjected to DOT1Li. As expected in both cell types, there was an almost complete loss of H3K79me1/2 upon DOT1Li (fig. S6C). However, we found opposite effects on the repressive and activating histone PTMs in MEFs and ESCs exposed to DOT1Li (Fig. 5A). While the repressive H3K27me3 increased by statistically significant levels in MEFs, a collection of histone acetylations found at the promoters of active genes were significantly increased only in ESCs (Fig. 5A and fig. S6, C and D). In contrast, exposure of MEFs or ESCs to histone deacetylase (HDAC) inhibitor SAHA increases histone acetylation but does not reciprocally decrease H3K79me2 (fig. S6E). Thus, DOT1L reduces repressive H3K27me3 or activating H3 and H4 acetylation marks, depending on the cell type.

In contrast to the cell type–specific effects, DOT1Li consistently increased both H3K27me3 (like somatic cells) and H3/H4 acetylation (like ESCs) during reprogramming (Fig. 5B and figs. S6, A and B, and S7, A and B). We confirmed that multiple histone acetylation marks were increased using small interfering RNA (siRNA) as an orthogonal approach to deplete DOT1L during reprogramming (fig. S7, C and E). None of the histone-modifying enzymes that have catalytic activity toward either H3K27 methylation or H3/H4 acetylation changed in RNA expression upon DOT1Li treatment during reprogramming (fig. S7F), although histone acetyltransferase (HAT) expression increases in ESCs. We note that the histone acetylations increased gradually from day 4 to day 6 (Fig. 5B and fig. S7B) when we start observing reprogrammed colonies. Thus, the increase in histone acetylation is likely to be a mixture of direct

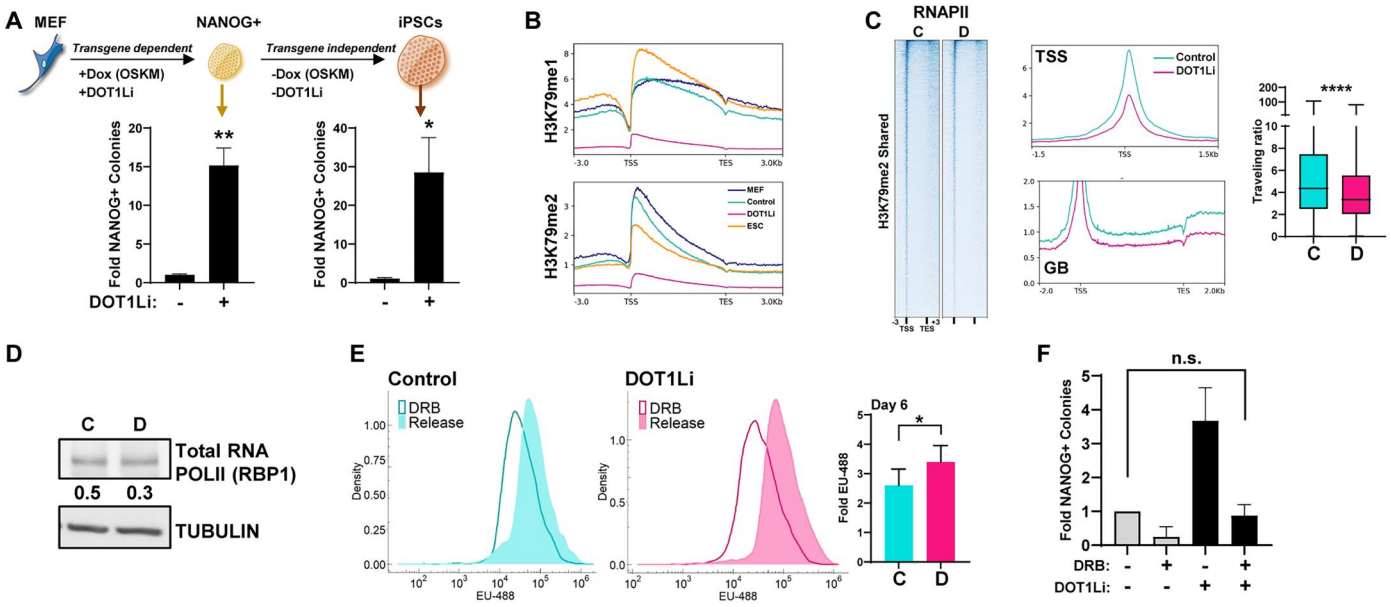

Fig. 4. Erasure of H3K79 methylation promotes reprogramming by altering RNAPII dynamics. (**A**) Top: Reprogramming scheme. OCT4, SOX2, KLF4, and c-MYC (OSKM) are induced in MEFs with doxycycline (Dox), and DOT1Li or DMSO control. Transgene-dependent colonies express NANOG in doxycycline on days 6 to 8. Transgene-independent colonies maintain NANOG expression after doxycycline and DOT1Li removal. Bottom: Reprogramming data are presented as the change relative to the control condition (set to 1). Bars are the mean + SD ($n = 3$). $^{**}P < 0.01$ and $^{*}P < 0.05$ by unpaired two-tailed t test. (**B**) Metaplots of H3K79me1/2 at H3K79me2-shared genes (Fig. 1A). (**C**) RNAPII at H3K79me2-shared genes in day 4 control (C)– and DOT1Li (D)–treated cells as RNAPII heatmap (left). Middle: RNAPII metaplots centered at the TSS or genebody (GB). Right: TR. Data are the mean ($n = 2$). $^{****}P < 0.0001$ by unpaired two-tailed t test. (**D**) Immunoblot of RNAPII on day 4 reprogramming of cells treated with control (C), or DOT1Li (D), quantitated relative to tubulin. (**E**) Left: Flow cytometry EU-488 signal density plot of day 6 of reprogramming cells treated with control or DOT1Li. Outline = unreleased cells; shaded = cells paused and then released for 30 min in the presence of EU. Right: Fold increase of EU-488 signal after release, DRB sample set to 1. Data are the mean + SD ($n = 3$). $^{*}P < 0.05$ by ratio paired two-tailed t test. (**F**) Reprogramming of cells treated with RNAPII inhibitor DRB, with and without DOT1Li, measured as transgene-dependent colonies. Colonies obtained in control condition set to 1. Bars are the mean + SD ($n = 3$). Not significant (n.s.) $P > 0.05$ by estimated marginal means on a mixed-effects model for a randomized complete block design with the Holm correction for multiple comparisons.

effects in early reprogramming cells and indirect effects when these early reprogramming cells begin expressing pluripotent levels of HATs.

While previous work has shown that H3K79me2/3 blocks the spread of H3K27me3 in leukemia by ChIP (*48*), a connection between H3K79 methylation and promoter histone acetylation is novel. Leukemia shares the infinite self-renewal phenotype of pluripotent stem cells. ESCs also have a hyperacetylated epigenome (*9*) that enables their open chromatin structure. Histone hyperacetylation is tightly connected to pluripotent identity as enforced maintenance of acetylation prevents differentiation (*49*). Therefore, an increase in either H3K27me3 or H3/H4 acetylations could potentially promote pluripotency. Hence, we sought to determine which of the two different classes of epigenetic alterations that we observed were functionally relevant to pluripotency acquisition (Fig. 5C).

H3K27me3 is deposited by the polycomb repressive complex 2, which includes the EED component that mediates the spread of H3K27me3 to adjacent histones. We measured the effect of EED inhibition (EEDi) in reprogramming in combination with DOT1Li (fig. S7G). Like our results above (Fig. 4A), DOT1Li increased reprogramming efficiency, while EEDi alone did not have any effect (Fig. 5D). However, when the DOT1Li and EEDi were combined, we found that reprogramming efficiency was modestly, but not significantly, increased in both OSKM-dependent NANOG^{+} colonies and fully reprogrammed transgene-independent iPSCs (Fig. 5D). Countering the DOT1Li-mediated H3K27me3 increase with EED inhibition did not reverse the enhanced reprogramming efficiency (Fig. 5D). Thus, DOT1Li-mediated H3K27me3 increase is detrimental to pluripotency acquisition through reprogramming.

Several different HATs are responsible for the individual histone acetylations that resulted from DOT1Li. Therefore, to interrogate the broad increase in histone acetylation (Fig. 5B and fig. S7B), we combined DOT1Li with the class I/II HDAC inhibitor SAHA to enhance retention of acetylation in the reprogramming population (Fig. 5E). The DOT1Li + SAHA combination did not cause any change in the number of OSKM-dependent NANOG^{+} colonies (Fig. 5F). Strikingly, upon withdrawal of doxycycline and small molecules, there was a significant increase in the OSKM transgene-independent stable iPSC in DOT1Li + SAHA–treated reprogramming populations (Fig. 5F and fig. S7H). DOT1Li induces a transient increase in H3/H4 acetylations, which are stabilized by using SAHA (Fig. 5E). Together, it is the retention of histone hyperacetylation triggered by the loss of H3K79me that specifically promotes transgene independence to generate bona fide iPSCs.

Reciprocal to the SAHA experiments, we tested the effects of inhibiting the H3K9 acetyltransferase GCN5 in the context of DOT1L inhibition (fig. S7I). Similar to depletion of GCN5 (*50*), its pharmacological inhibition with CPTH6 alone reduced both transgene-dependent and transgene-independent iPSC colonies (Fig. 5G). When the GCN5 inhibitor was combined with DOT1Li, the gain in both transgene-dependent and transgene-independent iPSC colonies

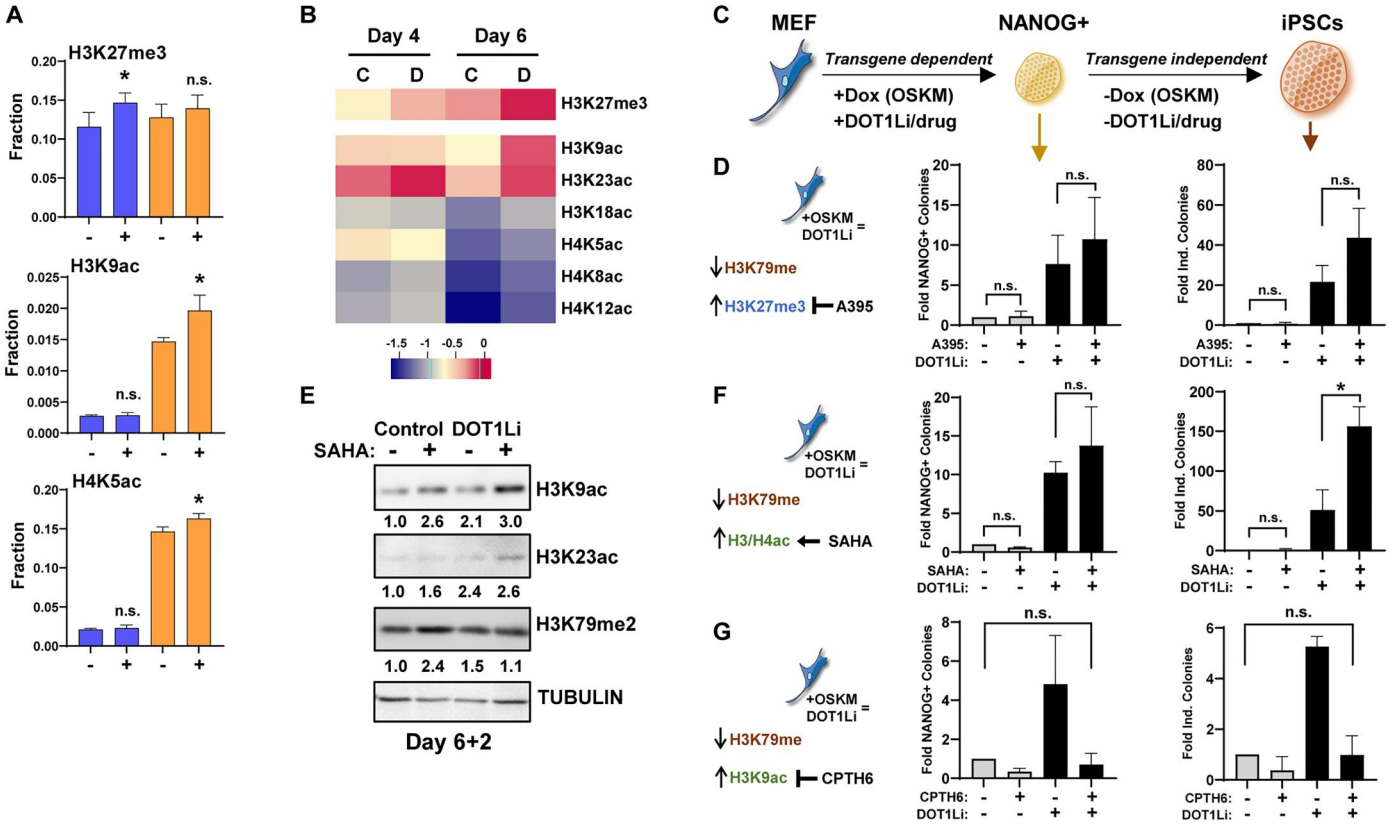

Fig. 5. Low DOT1L activity enables higher histone acetylation. (**A**) Average fraction of peptides containing the specified modification determined by mass spectrometry of MEFs (blue) or ESCs (orange) treated with control (−) or DOT1Li (+) for 4 days. Significance determined relative to control treatment of the same cell type. Data are the mean + SD ($n = 3$ to 4). *$P < 0.05$ or not significant (n.s.) $P > 0.05$ by unpaired two-tailed t test. (**B**) Log_2 fold change average peptide ratio heatmap of select modifications in control (C)– and DOT1Li (D)–treated reprogramming cells relative to the fraction modified in ESCs. Data are the mean ($n = 3$ to 4). (**C**) Reprogramming scheme of transgene-dependent and transgene-independent NANOG$^+$ colonies. (**D**, **F**, and **G**) Left: Schematic of histone modification targeting during reprogramming. Cells were treated with control (gray) or DOT1Li (black), with and without the specified small molecule—(D) EED inhibitor A395, (F) HDAC inhibitor SAHA, and (G) GCN5 inhibitor CPTH6—measured as transgene-dependent (middle) and transgene-independent (right) colonies. Colonies obtained in control condition set to 1. Bars are the mean + SD ($n = 3$). All unnormalized data are provided in fig. S7 and used for statistical testing. Not significant (n.s.) $P > 0.05$ and *$P < 0.05$ by estimated marginal means on a mixed-effects model for a randomized complete block design with the Holm correction for multiple comparisons. (**E**) Immunoblot 2 days after doxycycline and DOT1Li/SAHA removal (after 6 days of reprogramming) of H3K9ac, H3K23ac, and H3K79me2 in control or DOT1Li cells treated with SAHA or vehicle beginning on day 3 of reprogramming, relative to tubulin.

was compromised (Fig. 5G). We examined the connection of histone acetylation and nascent transcription on day 4 of reprogramming upon release from DRB-mediated pausing using intron qPCR. The GCN5 inhibitor decreased nascent transcription in the absence and presence of DOT1Li (fig. S7J). These results suggest that loss of H3K79me2 controls nascent transcription by modulating histone acetylation.

Similar to the GCN5 inhibitor CPTH6, the H4 acetyltransferase HBO1 inhibitor WM-3835 reduced the number of iPSCs (fig. S7K) (*51*). Since both CPTH6 and WM-3835 decrease iPSC colonies, we cannot rule out effects on general histone acetylation independent or the specific DOT1Li-mediated increase in histone acetylation. Nonetheless, these data indicate that hyperacetylation of both H3 and H4 residues contributes to the gain of pluripotency.

Inhibition of DOT1L increases H3K9ac at ubiquitously expressed genes that have shared H3K79me enrichment in both ESCs and MEFs

Since histone acetylation increases upon H3K79me loss, and DOT1Li-mediated reprogramming is counteracted by GCN5 inhibition, we investigated where the gain of H3K9ac was localized. We performed ChIP-seq for H3K9ac on day 4 of reprogramming treated with control or DOT1Li and compared it to locations in MEFs and ESCs. Similar to H3K79 methylation, H3K9ac is overwhelmingly localized to promoter and genic locations (fig. S8A). Over 60% of genes with H3K9ac enrichment were shared in all four conditions/cell types (fig. S8B). Only 131 genes gained H3K9ac peaks exclusively in the DOT1Li reprogramming condition (fig. S8B), demonstrating that DOT1Li does not result in H3K9ac being installed at new locations during reprogramming. Therefore, we quantitated the amount of H3K9ac in DOT1Li versus the control reprogramming population.

We compared the features of the genes that gained H3K9ac (top 10% increased) to the ones that lost H3K9ac (bottom 10%

decreased) as a control (Fig. 6A). The genes with the most increased H3K9ac upon DOT1Li shared H3K79me2 enrichment in both MEFs and ESCs rather than each cell type alone (Fig. 6B). In this shared subset, the H3K9ac-increased genes have significantly higher level of H3K79me2 and paused RNAPII than the H3K9ac-decreased genes in MEFs (Fig. 6C), more so than in ESCs (fig. S8C). The H3K9ac-increased genes are longer (fig. S8D) and have a longer first intron and more introns per gene (fig. S8E). They are also rapidly transcribed in ESCs (fig. S8F), but have a lower total level of expression in MEFs and ESCs (Fig. 6C and fig. S8C). There is a modest gain in expression of increased genes during reprogramming when cells are treated with DOT1Li, indicating that elevated H3K9ac leads to increased transcription (Fig. 6D). In contrast to the shared subset, there were no differences in the H3K79me2 levels between the H3K9ac-increased and H3K9ac-decreased genes in the exclusively MEF or ESC subset (fig. S8G). Thus, the effect of H3K79me2 loss at the mid-stages of reprogramming (day 4) is an increase of H3K9ac at non–lineage-specifying genes.

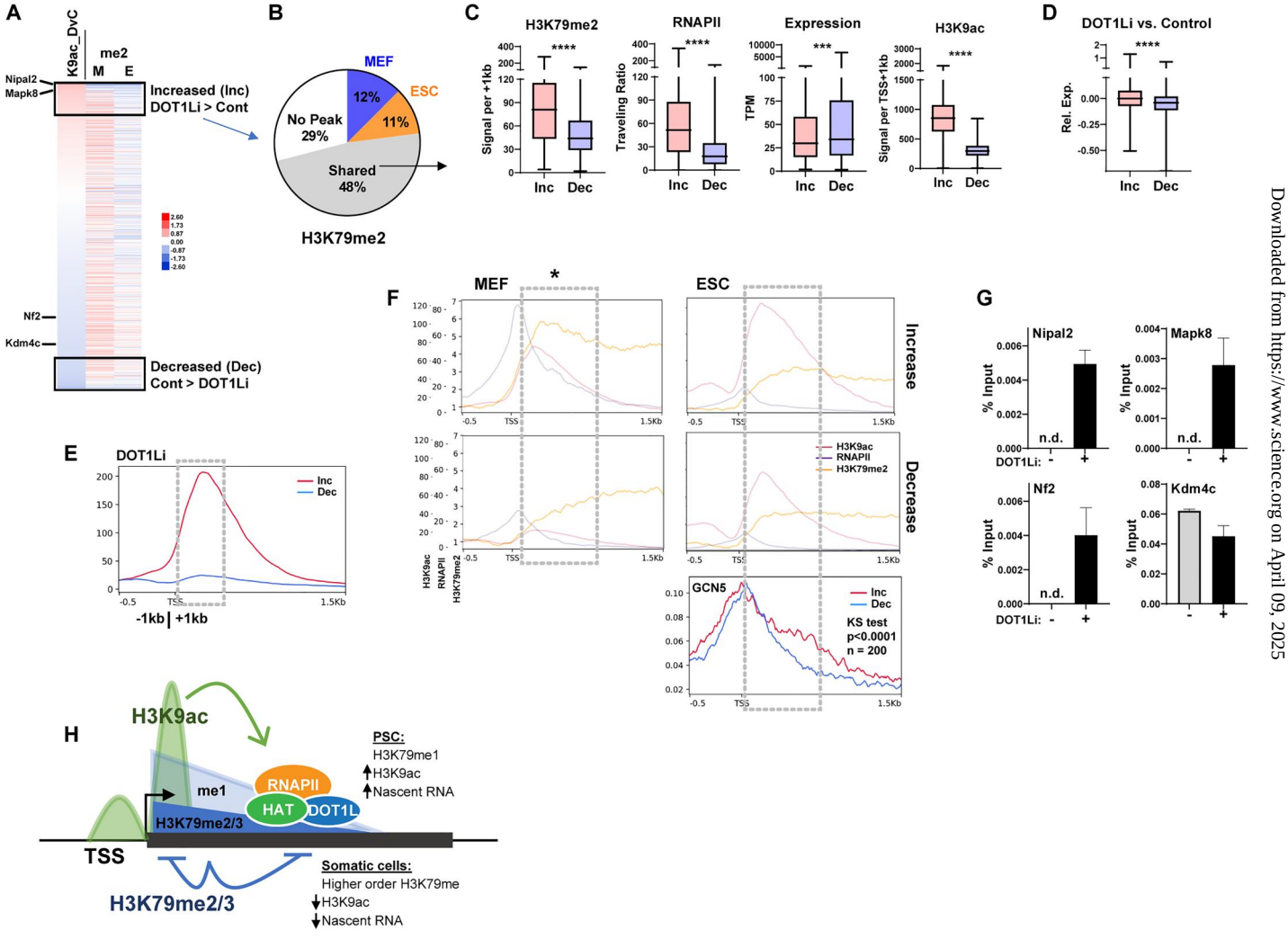

Fig. 6. Inhibition of DOT1L increases H3K9ac at ubiquitously expressed genes that have shared H3K79me enrichment in both ESCs and MEFs. (**A**) H3K79me2 (me2) heatmap of genes with an H3K9ac peak, sorted by relative H3K9ac in day 4 reprogramming DOT1Li (D) versus control (C). TSS to +1 kb quantitated. (**B**) H3K79me2 peak status of the top 10% of H3K9ac-increased (Inc) genes. (**C** to **F**) H3K79me2-shared genes, in H3K9ac-increased, compared to the bottom 10% with decreased (Dec) H3K9ac signal were isolated for analysis of (****$P < 0.0001$ and ***$P < 0.001$ by unpaired two-tailed t test) (C) MEF—H3K79me2 (TSS to +1 kb). RNAPII TR (TSS/genebody). Expression (TPM). H3K9ac (TSS to +1 kb). (D) Log_2 fold change in expression in DOT1Li relative to control on day 4 of reprogramming. (E) H3K9ac metaplot of day 4 reprogramming cells treated with DOT1Li. Area of increased H3K9ac boxed in gray (TSS to +1 kb). (F) H3K79me2 (orange), H3K9ac (red), and RNAPII (purple) metaplots. *Area of decreased H3K79me2/increased H3K9ac. Note relative enrichment depicted by y axes. Bottom: GCN5 metaplot in ESCs. Increased and decreased enrichment compared by Kolmogorov-Smirnov (KS) test. (**G**) GCN5 ChIP-qPCR of genes with H3K9ac [enrichment location labeled on (A)]. (**H**) Model: DOT1L is recruited to transcribing genes. ESCs have higher levels of RNAPII and lower levels of DOT1L correlating with a feed-forward loop of faster elongation and enrichment of H3K9ac downstream of the TSS. Somatic cells are more biased to RNAPII initiation/pause, detaining DOT1L at promoters, resulting in higher-order H3K79me2/3 as it is a distributive enzyme. Reduction of H3K79 methylation during reprogramming with DOT1Li allows establishment of ESC-like H3K9 acetylation and greater de novo transcription.

H3K79me2 and H3K9ac directly overlap proximal to the RNAPII pause site

In the DOT1Li reprogramming populations, we observed that H3K9ac increased specifically after the TSS (Fig. 6E). To investigate this change in pattern of H3K9ac further, we compared MEFs and ESC around the RNAPII pause site. In MEFs at locations where H3K9ac is increased by DOT1Li, the apex of H3K79me2 enrichment coincided with that of H3K9ac after the RNAPII pause site, but not at the H3K9ac-decreased locations (Fig. 6F). In contrast to the high H3K79me2/low H3K9ac in MEFs, ESCs had more elongating RNAPII coupled with a pattern of low H3K79me2/high H3K9ac. H3K9ac is a platform for recruiting the super elongation complex (SEC) (*52*) likely via the DOT1L-interacting protein AF9 (*53*–*55*). Combining DOT1L-KO ESCs with an SEC inhibitor affects transcriptional elongation especially at long genes (*21*). Therefore, DOT1Li treatment during reprogramming may switch the genes destined to have more elongating RNAPII to an ESC-like histone modification profile. We mapped previously published GCN5 ChIP-seq data in ESCs (*50*) onto the locations that increased or decreased in H3K9ac upon DOT1Li. GCN5 was significantly bound directly adjacent to the pause site, overlapping with the increase in H3K9ac, compared to the H3K9ac-decreased genes (Fig. 6F). We performed ChIP-qPCR for selected genes that either increased or decreased in H3K9ac (Fig. 6A). GCN5 was enriched at two locations that gained H3K9ac upon DOT1L inhibition but could also be gained or remain unchanged at the two decreased locations (Fig. 6G). Thus, while DOT1L inhibition has the potential to allow GCN5 binding, there are likely to be additional locus-specific determinants of the extent of GCN5 acquisition.

DISCUSSION

Our findings are consistent with a model where RNAPII elongation rates differ in somatic and pluripotent cell types, leading to distinct accumulation of nascent RNA. H3K79 methylation accumulates after transcription commences (*39*). In somatic cells, the greater residence time of RNAPII at the TSS prolongs DOT1L association (*56*), converting H3K79me1 to H3K79me2/me3 (Fig. 6H). By contrast, in ESCs, a combination of elevated RNAPII levels (Fig. 2B) and a less compacted chromatin environment likely facilitates RNAPII transition to transcriptional elongation that does not allow H3K79me2/me3 accumulation. During reprogramming, DOT1L inhibition mimics the ESC-like reduced H3K79me2/me3 and prompts a redistribution of RNAPII, which is accompanied by an increase in local histone acetylation modifications that facilitate elongation. Our findings implicate that DOT1L may provide a balance between transcription initiation and elongation during reprogramming.

Hypertranscription at essential genes (Fig. 3A) that form the building blocks of gene expression complexes and metabolic processes (such as *Sfpq*) may favor iPSC generation as pluripotent cells have greater biosynthetic needs due to their constant self-renewal (*12*, *57*). Thus, increased nascent transcription of non–lineage-specifying genes at the mid-point of reprogramming may propel iPSC formation at later stages. The presence of a pause regulatory step correlates with increased transcription (*11*), and highly transcribed essential housekeeping genes in particular are regulated by RNAPII pausing in ESCs (*58*). Notably, DOT1L does not affect the ability of RNAPII to enter a pause in ESCs (*21*). Efficient RNAPII elongation via the polymerase associated factor (PAF) complex is essential for pluripotency (*59*). Strikingly, DOT1L depletion can replace the reprogramming factor c-Myc (*27*) in the Yamanaka cocktail, which has a well-established role in pause release (*40*).

H3K9ac promotes pause release at candidate loci in HeLa cells by recruiting the SEC (*52*) likely through the reader AF9 that also associates with DOT1L (*53*–*55*). The post-TSS gain in H3K9ac could be due to decreased residence time of RNAPII and Spt5-Ada-Gcn5 acetyltransferase (SAGA) complex at the promoter region (*60*), or DOT1L presence may counter recruitment of the SAGA complex as observed in erythroleukemia cells (*61*). The phenomenon of DOT1L affecting pause release seems to be evolutionarily conserved since in *Caenorhabditis elegans*, the deletion of *Zfp-1*, the catalytic activator of Dot-1, increased transcriptionally engaged RNAPII by GRO-seq and reduced the pausing index (*62*).

DOT1L inhibition also endows a permissive state in which other POU domain–containing proteins can replace OCT4 in the Yamanaka cocktail (*63*). Beyond pause release, histone hyperacetylation (Fig. 5) may confer chromatin loosening for reprogramming factor binding at promoters of highly expressed genes in our report. Together, DOT1L plays a central role in altering nonpluripotent gene regulation to an ESC-like status during cell fate change.

Both cellular and locus-specific environments could further fine-tune DOT1L effects. DOT1L deletion reduces transcription initiation in MEFs subjected to ultraviolet damage (*64*), and in erythroleukemia cells (*61*) without increasing nascent transcription. H3K79me may participate in an alternative epigenetic networks in somatic cells by regulating spread of H3K27me3 (Fig. 4A) and H3K27ac (*48*, *65*–*69*).

Together, our data provide insights into a new facet of pluripotency that focus on histone modification dynamics within the gene bodies to regulate cell fate transitions, and open up new avenues for further improvement in reprogramming efficiency.

MATERIALS AND METHODS

Cell isolation and culture

Mice were maintained in agreement with our University of Wisconsin-Madison Institutional Animal Care and Use Committee (IACUC)–approved protocol. Male and female reprogrammable MEFs were isolated from embryos homozygous for the *Oct4*-2A-*Klf4*-2A-IRES-*Sox2*-2A-*c-Myc* (OKSM) transgene at the *Col1a1* locus and heterozygous for the reverse tetracycline transactivator (rtTA) allele at the *Rosa26* locus on embryonic day 13.5, as previously described (*70*). MEFs were cultured in MEF medium [Dulbecco's modified Eagle's medium (DMEM), 10% fetal bovine serum (FBS), 1× nonessential amino acids, 1× GlutaMAX, 1× penicillin/streptomycin, and 4 μl/500 ml of 2-mercaptoethanol]. Feeder MEFs were isolated at day E13.5 from DR4 embryos genetically resistant to geneticin (G418), puromycin, hygromycin, and 6-thioguanine. Feeder embryos were expanded for three passages and irradiated with 9000 rads. ESCs (V6.5 and E14) and iPSCs were cultured on gelatinized dishes with ESC medium (knockout DMEM, 15% FBS, 1× nonessential amino acids, 1× GlutaMAX, 1× penicillin/streptomycin, 4 μl/525 ml of 2-mercaptoethanol, and leukemia inhibitory factor). V6.5 ESCs and 2D4 iPSCs were grown on feeder MEFs. ESCs and iPSCs were MEF-depleted by incubation for 30 min in a nongelatinized dish before plating. Primary astrocytes were grown in DMEM with 1% FBS, 1× nonessential amino acids, 1× GlutaMAX, and 1× penicillin/streptomycin and isolated as previously described (*46*).

293T and normal human dermal fibroblasts were cultured in DMEM and 10% FBS and acquired from the American Type Culture Collection.

Inducible DOT1L ESC lines

A 5′-FLAG–tagged full-length mouse DOT1L cDNA sequence was cloned into pBS33, which was integrated with FLP recombinase into the *Col1a1* locus of V6.5, under the control of a doxycycline-inducible promoter (*71*). DOT1L expression was induced with doxycycline (2 μg/ml).

Pluripotency continuum state transition

E14 ESCs were maintained in feeder-free conditions with serum/LIF ESC medium (knockout DMEM, 15% FBS, 1× nonessential amino acids, 1× GlutaMAX, 1× penicillin/streptomycin, 4 μl/525 ml of 2-mercaptoethanol, and leukemia inhibitory factor) on 0.1% gelatin-coated plates. E14 cells were passaged with 0.25% trypsin. For 2i/LIF state, E14 serum/LIF ESCs were passaged two times on 0.1% gelatin-coated plates in modified 2i/LIF medium: 50% DMEM/F12 + N-2 supplement + insulin (12.5 mg/liter) + progesterone (0.01 mg/liter), 50% Neurobasal medium + B-27 minus vitamin A, LIF (1000 U/ml), 2-mercaptoethanol (6.3 μl/liter), penicillin-streptomycin, 3 μM CHIR-99021, 0.4 PD-032590, bovine serum albumin (BSA) (0.0025%), and 5% FBS. 2i/LIF ESCs were passaged with TrypLE. For formative stem cell culture, 2i/LIF E14 ESCs were plated on fibronectin-coated plates (16.6 μl/ml) in modified AloXR medium: 50% DMEM/F12, N-2 supplement, insulin (12.5 mg/liter), progesterone (0.01 mg/liter), 50% Neurobasal medium, B-27 minus vitamin A, 2-mercaptoethanol (6.3 μl/liter), penicillin-streptomycin, activin A (3 ng/ml), 2 mM XAV939, 1 mM BMS493, BSA (0.0025%), and 1% FBS. Formative condition cells were passaged five times with Accutase. Expression of genes up-regulated in formative or naïve conditions (*42*, *72*) was assessed by RT-qPCR (table S1).

Reprogramming

Reprogrammable MEFs were plated at a density of 30,000 to 50,000 cells per gelatinized 12-well at day 0. Reprogramming was initiated with doxycycline (2 μg/ml) in ESC medium containing dimethyl sulfoxide (DMSO) control or drug treatment. SGC0946 (DOT1Li) was used at 5 μM (ApexBio, A4167), vorinostat (SAHA) at 1 μM (Cell Signaling Technology, 12520S), CPTH6 hydrobromide at 40 μM (Cayman Chemical, 19828), DRB at 10 μM (Sigma-Aldrich, D1916), WM-3835 at 2 μM (MedChemExpress, HY-134901), and A-395 hydrochloride at 1 μM (Millipore Sigma, SML1923). Feeder MEFs were added at 50% confluency within days 0 to 2. The medium containing fresh drugs and doxycycline was changed every 48 hours until efficiency was measured by immunofluorescence for the pluripotency factor NANOG. Days 6 to 8 were chosen as the endpoint as reprogramming proceeded long enough for stable colony formation, but not so long that cells became overcrowded in SGC0946 (DOT1Li) treatment. OSKM-independent colonies were assessed by removing doxycycline and drugs for 2 to 4 days followed by immunofluorescence for sustained NANOG expression. A reprogrammed colony was considered as a grouping of at least four $NANOG^+$ cells.

Reprogramming statistical analysis

At least three biological replicate experiments consisting of independent MEF isolations and/or days of treatment were performed for each reprogramming figure. Biological replicate information is included in all figure legends, and all individual biological replicate primary data are shown in supplementary figures. Each biological replicate was the average of at least two technical replicate wells, and the treatments and biological replicates together comprised a randomized complete block design with blocking on the biological replicates. Data were assessed for normality with the Shapiro-Wilk test, and homogeneity of variances with the Fligner-Killeen test. If both conditions were met, significance was assessed using an analysis of variance (ANOVA) on a two-way mixed-effects model (R package lme4) with one fixed effect (treatment) and one random effect (MEF isolation), when comparing more than two groups. Following significance determination, the model residuals were assessed for normality using the Shapiro-Wilk test. Group comparisons were made using estimated marginal means (R package emmeans) for the fixed effect in the model and using the Holm adjustment method to account for multiple group comparisons. When only two groups were compared, the comparisons were performed in GraphPad Prism 9 using two-tailed *t* tests, as specified in legends. All reprogramming experiment significance and *P* values are explained in legends. Figures were generated using GraphPad Prism 9. Data are plotted as the mean of the biological replicates, with the control condition set to 1. Error bars depict the SD of the biological replicates.

Immunofluorescence

Coverslips were fixed in 4% paraformaldehyde/phosphate-buffered saline (PBS), permeabilized in 0.5% Triton-X/PBS, and washed in 0.2% Tween 20/PBS for 10 min each. Coverslips were blocked in blocking buffer (5% goat serum, 1× PBS, 0.2% Tween 20, 0.2% fish skin gelatin) for 30 min. Coverslips were stained with anti-NANOG (1:1000; Cell Signaling Technology, 8822S) in blocking buffer for 1 hour and then washed twice in wash buffer. Coverslips were stained with secondary goat anti–immunoglobulin G (IgG)–DyLight 488 (1:1000; Thermo Fisher Scientific, 35552) in blocking buffer for 1 hour. Coverslips were washed 1× in wash buffer, 1× in wash buffer containing 4′,6-diamidino-2-phenylindole dihydrochloride (0.1 μg/ml) (Millipore Sigma, D8417), and 1× in wash buffer for 5 min each, before mounting on slides with aqua-polymount (Fisher Scientific, NC9439247). Counts and imaging were performed on Nikon Eclipse Ti using NIS Elements software.

siRNA transfection

Cells were transfected every 48 hours in 0.5 ml per 12-well. DharmaFECT 1 (1 μl) (Fisher Scientific, T200104) was diluted in 49 μl of serum-free DMEM and incubated for 5 min. The transfection reagent was then added to siRNA in 50 μl of serum-free DMEM and allowed to incubate for 20 min. Cells were transfected with 20 nmol of siRNA on days 0 and 2 of reprogramming and then with 40 nmol on day 4 to account for increased cell number. siRNA was purchased from Dharmacon (horizon): si*Dot1l* (J-057964-12) and nontargeting control (D-001810-01).

Reverse transcription qPCR

RNA was isolated from cells with the Isolate II RNA Mini Kit (Bioline, BIO-52702). One microgram was converted to cDNA

with qScript (Quanta, 95047), and 20 ng of cDNA (based on the original RNA concentration) was used for qPCR analysis in 10-μl reactions with SYBR Green (Bio-Rad, 1725124) (table S1). cDNA was diluted 1:500 to measure RNAPI transcripts. Expression was calculated relative to one or the geometric mean of the two housekeeping genes.

Immunoblot

Cells were lysed in SUMO buffer: $^{1}/_{4}$ part I [5% SDS, 0.15 M tris-HCl (pH 6.8), 30% glycerol], $^{3}/_{4}$ part II [25 mM tris-HCl (pH 8.3), 50 mM NaCl, 0.5% NP-40, 0.5% deoxycholate, 0.1% SDS], and 1× cOmplete protease inhibitors (Roche, 4693132001). Lysates were sonicated with a microtip for 5 s at 20% amplitude and quantitated in DC Protein Assay Kit II (Bio-Rad, 5000112) against a BSA standard curve. Twenty-five micrograms was loaded for H3K79me1/2 blots, 30 μg for RNAPII blots, 10 μg for acetylation blots, and 10 μg for H3K27me3. Protein was transferred to a nitrocellulose membrane and blocked in 5% milk/PBS–0.1% Tween 20 for 30 min. Membranes were probed for 1 hour to overnight in primary antibody, including H3K79me1 (1:1000; Diagenode, C15410082 or Abcam, ab2886), H3K79me2 (1:1000; Active Motif, 39143), H3K79me3 (1:1000; Diagenode, C15410068), H3K9ac (1:1000; Active Motif, 39917), H3K23ac (1:1000; Active Motif, 39131), H3K27me3 (1:1000; Cell Signaling, 9733S), RNAPII RPB1 NTD D8L4Y (1:1000; Cell Signaling, 14958S), total H3 (1:3000; Cell Signaling, 3638S), and α-tubulin (1:3000; Cell Signaling, 3873). Membranes were washed twice in wash buffer (PBS, 0.1% Tween 20) and incubated with secondary antibody for 1 hour. Membranes were washed three times in wash buffer and imaged with ECL on ImageQuant LAS 4000 or with a LI-COR Odyssey imaging system. Tiff files were quantitated with Image Studio Lite V5.2 using the Add Rectangle function.

Histone acid extraction and mass spectrometry

Two independent biological replicate expansions, each consisting of four technical replicates, were analyzed. Four million cells were resuspended in 800 μl of buffer A [10 mM tris (pH 7.4), 10 mM NaCl, 3 mM $MgCl_2$] containing fresh 10 mM nicotinamide, 1 mM sodium butyrate, 4 μM trichostatin A, and 1× protease inhibitor (Roche, 4693132001) and transferred to a dounce homogenizer. Nuclei were isolated with 60 strokes using a tight pestle. The dounce was washed with 200 μl of buffer A and combined to make a total of 1 ml of lysate, which was centrifuged at 800*g* for 10 min at 4°C. The nuclei pellet was washed twice in cold PBS and spun as above. The pellet was resuspended in 500 μl of 0.4 N H_2SO_4 and rotated for 4 hours at 4°C. Tubes were then spun at 3400*g* for 10 min at 4°C, and the supernatant containing histones was isolated. One hundred twenty-five microliters of 100% trichloroacetic acid was added and incubated overnight. Histones were precipitated by centrifugation at 3400*g* for 5 min at 4°C and washed twice with 100% ice-cold acetone. The pellet was air-dried for 4 hours and then resuspended in 100 μl of H_2O. The solution was centrifuged at 3400*g* for 2 min, and the supernatant was collected. Protein concentration was measured against a standard curve with DC Protein Assay Kit II (Bio-Rad, 5000112) assay. Protein (5 μg) was dried by SpeedVac and prepared for mass spectrometry as previously described (*73*). Peptides were analyzed with Epiprofile 2.0 (*74*).

ChIP and library

At least 5× 15 cm of MEFs, 2× 15 cm of ESCs, and 4× 15 cm of reprogramming day 4 cells were used as starting material. Each ChIP was performed on a separate biological replicate expansion, and duplicates were immunoprecipitated on separate days (Table 1). Cells were trypsinized and fixed with 1% formaldehyde in suspension for 10 min, rotating. Cross-linking was quenched with 0.14 M glycine for 5 min, cells were centrifuged at 300*g* for 3 min, and pellets were washed three times with cold 1× PBS. Cells (25 million) were resuspended in 1 ml of lysis buffer [1% SDS, 50 mM tris-HCl (pH 8), 20 mM EDTA, 1× cOmplete (Roche, 4693132001) protease inhibitor] and sonicated on a Covaris S220 Focused-ultrasonicator with the following parameters: 21 cycles of 45 s ON (peak 170, duty factor 5, cycles/burst 200), 45 s OFF (rest) in 6° to 8°C degassed water. Aliquots (25 μl) were taken at 0, 10, and 21 cycles to check DNA fragmentation. Aliquots were diluted with 75 μl of H_2O and incubated with 10 μg of ribonuclease (RNase) for 30 min at 37°C. One microliter of proteinase K (20 mg/μl) was added, and sonication samples were incubated at 60°C overnight to reverse crosslinks. DNA was purified with phenol-chloroform extraction with phase lock tubes, precipitated with isopropanol, and run on a 1.5% agarose gel to ensure generation of 200- to 400-bp fragments.

Sonicated chromatin was centrifuged at 21,000*g* at 6°C for 10 min, and supernatant was collected and quantified with the Qubit DNA HS Assay Kit (Thermo Fisher Scientific, Q32854). Chromatin was aliquoted ensuring that the SDS remained in solution so that the concentration was exactly 0.1% after diluting 1:10 in dilution buffer [16.7 mM tris-HCl (pH 8), 0.01% SDS, 1.1% Triton-X, 1.2 mM EDTA, and 167 mM NaCl]. H3K79me1/2/3 ChIPs started with 7.1 μg of chromatin combined with 1/53 (134 ng) human spike-in chromatin generated from 293T cells as above (*31*). H3K9ac and RNAPII ChIP-seqs were immunoprecipitated with 13 μg of chromatin with 1/53 (247 ng) human spike-in generated from human dermal fibroblasts for H3K9ac or 293T cells for RNAPII. GCN5 ChIP was performed with 16 μg of chromatin. ChIP-qPCR experiments were quantitated relative to input dilutions (not spike-in). Five micrograms (or 5 μl if concentration was unknown) of the following antibodies was used: H3K79me1 (Abcam, 2886), H3K79me2 (Active Motif, 39143), H3K79me2 (Abcam, ab3594), H3K79me3 (Diagenode, C15410068), H3K9ac (Diagenode, pAb-004-050 Rep 1, 293T spike in control), H3K9ac (Active Motif, 39917, Reps 2-3 dermal fibroblast control), RPB1 NTD D8L4Y (Cell Signaling Technology, 14958S), and GCN5 (Santa Cruz Biotechnology, sc-20698).

ChIPs were incubated overnight at 4°C with rotation, and then Dynabeads were added for 2 hours. Dynabeads were pre-prepared as follows: 25 μl of protein A (Thermo Fisher Scientific, 10002D) and 25 μl of protein G (Thermo Fisher Scientific, 10004D) were combined and washed once in PBS, 0.02% Tween 20 and once in dilution buffer, and then resuspended in an equal volume of dilution buffer. Antibody-bead complexes were washed twice for 5 min rotating at 4°C in 1 ml of each of the following buffers: low salt [50 mM Hepes (pH 7.9), 0.1% SDS, 1% Triton X-100, 0.1% deoxycholate, 1 mM EDTA (pH 8.0), 140 mM NaCl], high salt [50 mM Hepes (pH 7.9), 0.1% SDS, 1% Triton X-100, 0.1% deoxycholate, 1 mM EDTA (pH 8.0), 500 mM NaCl], LiCl [20 mM tris-HCl (pH 8), 0.5% NP-40, 0.5% deoxycholate, 1 mM EDTA (pH 8.0), 250 mM LiCl], and TE [10 mM tris-HCl (pH 8), 1 mM EDTA (pH 8)]

Table 1. ChIP-seq sample information.

Antibody	Sample	Total reads	Mouse reads	Human reads	Scaling factor	Pearson correlation
			H3K79me1			
ab2886	MEF1	40768134	34615651	847674	1.99	0.94
ab2886	MEF2	38425323	30464003	721201	2.34	
ab2886	ESC1	42297298	38941623	1428991	1.18	0.80
ab2886	ESC2	45381584	37335281	849441	1.99	
ab2886	Control1	26820824	23755925	946357	1.78	0.89
ab2886	Control2	43783616	35153412	925777	1.82	
ab2886	DOT1Li1	41021137	35959503	4494203	0.38	0.88
ab2886	DOT1Li1	36464932	30622064	4164031	0.41	
			H3K79me2			
39143	MEF1	38863176	31032385	957631	1	0.82
39143	MEF2	34764245	32302636	603358	1.59	
39143	ESC1	34928516	31936040	1439224	0.67	0.89
39143	ESC2	40015359	37718191	1590420	0.60	
39143	Control1	42997663	39198790	1551862	0.62	0.91
ab3594	Control2	38083981	33522749	1076055	0.89	
39143	DOT1Li1	37560027	32661020	3766380	0.25	0.87
ab3594	DOT1Li1	38113067	33248456	3349534	0.29	
			H3K79me3			
C15410068	MEF1	42663038	36042196	658250	1	0.90
C15410068	MEF2	36525240	31915808	594060	1.11	
C15410068	ESC1	43201707	37759562	957609	0.69	0.72
C15410068	ESC2	50440669	47877283	1315107	0.50	
C15410068	Control1	44389104	39581481	3110931	0.21	0.86
C15410068	Control2	41270897	37746008	940561	0.70	
C15410068	DOT1Li1	30543411	25549829	3372288	0.20	0.92
C15410068	DOT1Li1	41225758	36976091	1965063	0.33	
			H3K9ac			
39917	MEF1	42230796	31615042	898447	1	0.80
pAb-004-050	MEF2	37819770	8724215	27613799	NA	
39917	ESC1	43216029	41411494	372117	2.41	0.83
pAb-004-050	ESC2	30996016	13140146	16791695	NA	
39917	Control1	40733343	37902670	474560	1.89	0.88
pAb-004-050	Control2	38215750	16669425	16272034	NA	
39917	Control3	27931443	26763906	248410	1	
39917	DOT1Li1	42363490	34183929	505729	1.78	0.90
pAb-004-050	DOT1Li2	39345786	13438879	24425255	NA	
39917	DOT1Li3	29366869	27406724	289010	0.86	
			RNA polymerase II			
14958S	MEF1	24120272	20106097	638534	1	0.95
14958S	MEF2	27669865	24113481	1983779	1	
14958S	ESC1	35949086	32434085	537669	1.19	1.0
14958S	ESC2	30896119	27217011	1763507	1.12	
14958S	Control1	36890695	34848591	683001	0.93	1.0
14958S	Control2	39739103	36440528	1893724	1.05	

continued on next page

Antibody	Sample	Total reads	Mouse reads	Human reads	Scaling factor	Pearson correlation
14958S	DOT1Li1	39627274	37284143	921804	0.69	1.0
14958S	DOT1Li1	39407753	35842510	2328380	0.85	

using a magnetic rack. Beads were incubated with 250 μl of elution buffer [50 mM tris-HCl (pH 8), 1 mM EDTA (pH 8), 1% SDS] plus 200 μl of TE with 0.67% SDS for 10 min at 65°C, shaking. RNase A (10 μg) was added and incubated at 37°C for 30 min. Crosslinks were reversed overnight with 40 μg of proteinase K at 63°C. DNA was purified with phenol-chloroform extraction with phase lock tubes followed by isopropanol precipitation. DNA was resuspended in ultrapure H_2O.

For sequencing experiments, the entire ChIP was concentrated to 5 μl with a SpeedVac and used for library preparation with Ovation Ultralow System V2 (NuGEN, 0344) according to the manufacturer's instructions. All reactions were performed in 0.5× the volume, and adapters were diluted 1:5 in water. Libraries were amplified for 10 cycles, and signal was checked by running 10% on 1.5% agarose gel before the final bead purification. After bead purification, the remaining library was run on a 1.5% agarose gel, and an additional size selection was performed by cutting from 200 to 400 bp. The library was purified with the MinElute Gel Extraction Kit (Qiagen, 28604). Quality was checked with the DNA HS Assay Kit (Thermo Fisher Scientific, Q32854) and Bioanalyzer3.0. Libraries were sequenced 1 × 50 on Illumina HiSeq4000 at the NUSeq Core (Northwestern Feinberg School of Medicine). GCN5 and RNAPII libraries (amplified 16 cycles) were used for qPCR analysis (table S2).

ChIP-seq analysis

Reads were aligned to the mm9 genome assembly using Bowtie2 (*75*). Sam files were converted into bam files with Samtools-1.2 (*76*) view. Bam files were sorted with Samtools-1.2 sort. Reads that did not align to the mouse genome were isolated from sorted bam files with Sam-1.2 view -f4. These unaligned bam files were converted into fastq files with Samtools-1.2 bam2fq. The fastq files were then aligned to the human hg19 assembly and processed to sorted bam files as above. The number of reads that unambiguously aligned to the human genome was quantified from the sorted bam files with Samtools-1.2 flagstat and used to calculate ChIP-seq scaling factors (see Table 1).

Peaks were called using MACS2 (*77*) callpeak. All ChIP-seqs were processed with both default and broad peak calling algorithms, with *P* values of 1×10^{-3} and 1×10^{-4}, which were assessed in Integrative Genomics Viewer (IGV) (*78*). H3K79me1/2/3 ChIP-seqs were called with --broad -p 0.0001, and H3K9ac narrow peaks were called with -p 0.001. Peak files were annotated to the mm9 genome with HOMER (*79*) annotatePeaks.pl. The output summary file was used to generate the percent genomic annotation stacked bar graphs. To determine genic lists for H3K79me ChIPs, genes with peaks within the gene body [5′ untranslated region (UTR), exon, intron, 3′UTR, and/or TTS] were isolated, and ChIP-seq sample replicates were overlapped using Venny2.0 to identify high-confidence consensus genes. To identify cell type–specific H3K79me genic lists, the high-confidence lists were overlapped using Venny2.0 and annotation was checked with Deeptools (*80*) *k*-means clustering of heatmaps. To generate gene-associated lists for H3K9ac, genes with peaks within the gene body and/or the promoter were isolated, and ChIP-seq sample replicates were overlapped using Venny2.0 to identify high-confidence consensus genes. The high-confidence consensus cell-specific gene lists were compared in a four-way Venn using the R package ggVennDiagram(x, label_alpha = 0, label = "count") + scale_fill_gradient. Gene ontology (GO) was performed with HOMER findMotifs.pl using the biological_process output or DAVID (https://david.ncifcrf.gov/tools.jsp) Functional Annotation Tool, Gene Ontology GOTERM_BP_4 and GOTERM_MF_4.

Deeptools was used to create heatmaps and metaplots. First, normalized bigwig files were generated using the command bamCoverage with the following parameters: --binSize 10 --scaleFactor (see Table 1) --ignoreForNormalization chrX. Matrices of normalized signal were created with the Deeptools computeMatrix command. In the case of H3K79me plots, the parameters were as follows: scale-regions -b 3000 -a 3000 --regionBodyLength 5000. For H3K9ac/RNAPII/GCN5 plots, the parameters were as follows: reference-point --referencePoint TSS -b 500 -a 1500, or as listed. Deeptools was used to compare normalized signal of ChIP-seq replicates by Pearson correlation with multiBigwigSummary -bs 1000. IGV was used to display example ChIP-seq tracks of normalized bigwig files. Reads over genomic coordinates were quantitated with BEDtools2.0 (*81*) multibamCov. Reads were normalized with the human spike-in scaling factor (see Table 1). In the case of H3K79me ChIP-seqs, scaled reads were further normalized to kb of gene length. To capture the DOT1Li-specific patterns in H3K9ac and H3K79me1/2/3, we quantitated signal from TSS to +1 kb downstream (Fig. 5A). TR was calculated by quantitating reads within the pausing region (from −30 to +300) and the elongation region (from +300 to transcription termination site) as previously described (*40*). Reads were normalized to the length (kb) of the assessed region. The TR was calculated as the length normalized pause signal divided by the elongation signal, and averaged between the two quantitated replicate ChIP-seqs per gene. H3K79me1/2/3 reads at the pause site (−30 to +300) were quantitated for comparisons to TR. All box and whisker plots were generated in GraphPad Prism as the box limits (25th to 75th percentiles), the center line (median), and the whiskers (minimum and maximum values). The mean is indicated with "+" as described in legends. Kolmogorov-Smirnov (KS) test of GCN5 ChIP enrichment was performed with GraphPad Prism with average GCN5 signal of 50-bp bins between H3K9ac-increased/H3K9ac-decreased genes −500-bp to +1500-bp region.

Nascent RNA EU profiling

Cells were treated for 2 hours and 50 min in 100 μM DRB alone, and then the medium was changed to contain DRB with EU (Click Chemistry Tools, 1261 and Thermo Fisher Scientific, E10345). EU quantity was scaled based on cell number with a minimum

concentration of 0.5 mM. After 10 min (3 hours total of DRB), the 0 time point was collected. For the transcriptional release time point, cells were washed twice in an excess of warm PBS to remove DRB, the medium with the scaled quantity of EU (and doxycycline/drugs if in use) was replaced, and cells were collected 30 min after DRB removal. If RNAPI was inhibited, cells were treated 30 min before release, and during release with 10 μM CX-5461 (ApexBio, A8337).

Nascent RNA was assessed in MEFs, in ESCs, and, on day 6 of reprogramming, with DMSO or SGC0946 (DOT1Li) as previously described (*82*) either in tubes for flow cytometry or on coverslips for microscopy imaging. The click reaction was performed for 1 hour in click staining solution [100 mM tris (pH 8.5), 1 mM $CuSO_4$, 2 μM AZDye-488 Azide (Click Chemistry Tools, 1275-1), and 100 mM ascorbic acid]. The Attune Flow Cytometer (Flow Cytometry Laboratory, University of Wisconsin Carbone Cancer Center Support Grant P30 CA014520) or the BD Accuri C6 Flow Cytometer was used to analyze 10,000 cells per sample, which were assessed using FlowJo software. Single cells were gated for analysis, and per-cell fluorescence was examined by exporting the scale values in FlowJo.

EU per nuclei was quantitated by imaging cells on coverslips. Cells were treated as above to label with EU-488. Images were captured on a Nikon Eclipse Ti using NIS Elements software, keeping exposure time consistent across cell types and coverslips. Pixel intensity of microscopy images was quantitated using FIJI. Tiff files were converted to RGB, and channels were split to isolate EU staining. Nuclei were captured with the lasso tool. The threshold was adjusted so the entire nucleus was selected and then measured.

To profile nascent transcripts by qPCR, MEFs, ESCs, and 2D4 iPSCs were counted and harvested in TRIzol. Drosophila S2 cells that had been treated for 2 hours with 2 mM EU were spiked in at a ratio of 1:20 (fly:mouse cells) for per-cell normalization. RNA was isolated with the RNA Clean & Concentrator-25 Kit (Zymo Research, R1018). The Click-iT Nascent RNA Capture Kit (Thermo Fisher Scientific, C10365) was used according to the manufacturer's instructions to pull down nascent EU-containing transcripts from 10 μg of starting total RNA. RNA was converted to cDNA from beads using qScript (Quanta, 95047) in 20-μl reactions. cDNA was diluted 1:4, and 1 μl was assessed by qPCR in 10-μl reactions. The Delta-Delta Ct was calculated relative to *Drosophila* spike in, setting unreleased MEFs (treated for 3 hours with DRB) to 1. Primers were designed within introns at the indicated genic position downstream of the TSS (table S2).

Nascent RNA intron profiling

Cells were treated for 3 hours with 100 μM DRB to pause transcription. Cells were washed twice in an excess of warm PBS to remove DRB, and the medium containing doxycycline and/or drugs (DMSO/SGC/CPTH6) was replaced. Transcription was released for 15 min. DRB paused and relased cells were collected with TRIzol. The aqueous layer was extracted with $^1/_5$ volume chloroform, and RNA was isolated with RNA Clean & Concentrator-25 (Zymo Research, R1017). Primers at least 2 kb from the TSS within an intron were used to profile nascent transcripts (table S2).

Other datasets

RNA-seq data GSE160580 was processed as previously described (*28*). ESC gene rates were from Fig. 3, source data 1 (12.5 to 25 min) (*83*). Other datasets were listed in table S3.

Supplementary Materials

This PDF file includes:

Figs. S1 to S8
Tables S1 to S3

REFERENCES AND NOTES

1. F. Spitz, E. E. M. Furlong, Transcription factors: From enhancer binding to developmental control. *Nat. Rev. Genet.* **13**, 613–626 (2012).
2. M. Levine, E. H. Davidson, Gene regulatory networks for development. *Proc. Natl. Acad. Sci. U.S.A.* **102**, 4936–4942 (2005).
3. T. Vierbuchen, A. Ostermeier, Z. P. Pang, Y. Kokubu, T. C. Südhof, M. Wernig, Direct conversion of fibroblasts to functional neurons by defined factors. *Nature* **463**, 1035–1041 (2010).
4. K. Takahashi, S. Yamanaka, Induction of pluripotent stem cells from mouse embryonic and adult fibroblast cultures by defined factors. *Cell* **126**, 663–676 (2006).
5. J. Brumbaugh, B. Di Stefano, K. Hochedlinger, Reprogramming: Identifying the mechanisms that safeguard cell identity. *Development* **146**, dev182170 (2019).
6. K. Hochedlinger, R. Jaenisch, Induced pluripotency and epigenetic reprogramming. *Cold Spring Harb. Perspect. Biol.* **7**, a019448 (2015).
7. B. Papp, K. Plath, Epigenetics of reprogramming to induced pluripotency. *Cell* **152**, 1324–1343 (2013).
8. A. Gaspar-Maia, A. Alajem, E. Meshorer, M. Ramalho-Santos, Open chromatin in pluripotency and reprogramming. *Nat. Rev. Mol. Cell Biol.* **12**, 36–47 (2011).
9. R. Sridharan, M. Gonzales-Cope, C. Chronis, G. Bonora, R. McKee, C. Huang, S. Patel, D. Lopez, N. Mishra, M. Pellegrini, M. Carey, B. A. Garcia, K. Plath, Proteomic and genomic approaches reveal critical functions of H3K9 methylation and heterochromatin protein-1γ in reprogramming to pluripotency. *Nat. Cell Biol.* **15**, 872–882 (2013).
10. S. Efroni, R. Duttagupta, J. Cheng, H. Dehghani, D. J. Hoeppner, C. Dash, D. P. Bazett-Jones, S. Le Grice, R. D. G. McKay, K. H. Buetow, T. R. Gingeras, T. Misteli, E. Meshorer, Global transcription in pluripotent embryonic stem cells. *Cell Stem Cell* **2**, 437–447 (2008).
11. I. M. Min, J. J. Waterfall, L. J. Core, R. J. Munroe, J. Schimenti, J. T. Lis, Regulating RNA polymerase pausing and transcription elongation in embryonic stem cells. *Genes Dev.* **25**, 742–754 (2011).
12. M. Percharde, A. Bulut-Karslioglu, M. Ramalho-Santos, Hypertranscription in development, stem cells, and regeneration. *Dev. Cell* **40**, 9–21 (2017).
13. E. E. Duffy, D. Canzio, T. Maniatis, M. D. Simon, Solid phase chemistry to covalently and reversibly capture thiolated RNA. *Nucleic Acids Res.* **46**, 6996–7005 (2018).
14. A. Veloso, K. S. Kirkconnell, B. Magnuson, B. Biewen, M. T. Paulsen, T. E. Wilson, M. Ljungman, Rate of elongation by RNA polymerase II is associated with specific gene features and epigenetic modifications. *Genome Res.* **24**, 896–905 (2014).
15. Z. Wang, C. Zang, J. A. Rosenfeld, D. E. Schones, A. Barski, S. Cuddapah, K. Cui, T.-Y. Roh, W. Peng, M. Q. Zhang, K. Zhao, Combinatorial patterns of histone acetylations and methylations in the human genome. *Nat. Genet.* **40**, 897–903 (2008).
16. H. Vlaming, F. van Leeuwen, The upstreams and downstreams of H3K79 methylation by DOT1L. *Chromosoma* **125**, 593–605 (2016).
17. E. J. Chory, J. P. Calarco, N. A. Hathaway, O. Bell, D. S. Neel, G. R. Crabtree, Nucleosome turnover regulates histone methylation patterns over the genome. *Mol. Cell* **73**, 61–72.e3 (2019).
18. D. De Vos, F. Frederiks, M. Terweij, T. van Welsem, K. F. Verzijlbergen, E. Iachina, E. L. de Graaf, A. F. M. Altelaar, G. Oudgenoeg, A. J. R. Heck, J. Krijgsveld, B. M. Bakker, F. van Leeuwen, Progressive methylation of ageing histones by Dot1 functions as a timer. *EMBO Rep.* **12**, 956–962 (2011).
19. W. Michowski, J. M. Chick, C. Chu, A. Kolodziejczyk, Y. Wang, J. M. Suski, B. Abraham, L. Anders, D. Day, L. M. Dunkl, M. L. C. Man, T. Zhang, P. Laphanuwat, N. A. Bacon, L. Liu, A. Fassl, S. Sharma, T. Otto, E. Jecrois, R. Han, K. E. Sweeney, S. Marro, M. Wernig, Y. Geng, A. Moses, C. Li, S. P. Gygi, R. A. Young, P. Sicinski, Cdk1 controls global epigenetic landscape in embryonic stem cells. *Mol. Cell* **78**, 459–476.e13 (2020).
20. B. Jones, H. Su, A. Bhat, H. Lei, J. Bajko, S. Hevi, G. A. Baltus, S. Kadam, H. Zhai, R. Valdez, S. Gonzalo, Y. Zhang, E. Li, T. Chen, The histone H3K79 methyltransferase Dot1L is essential for mammalian development and heterochromatin structure. *PLOS Genet.* **4**, e1000190 (2008).
21. K. Cao, M. Ugarenko, P. A. Ozark, J. Wang, S. A. Marshall, E. J. Rendleman, K. Liang, L. Wang, L. Zou, E. R. Smith, F. Yue, A. Shilatifard, DOT1L-controlled cell-fate determination and transcription elongation are independent of H3K79 methylation. *Proc. Natl. Acad. Sci. U.S.A.* **117**, 27365–27373 (2020).

22. Y. Xu, J. Zhao, Y. Ren, X. Wang, Y. Lyu, B. Xie, Y. Sun, X. Yuan, H. Liu, W. Yang, Y. Fu, Y. Yu, Y. Liu, R. Mu, C. Li, J. Xu, H. Deng, Derivation of totipotent-like stem cells with blastocyst-like structure forming potential. *Cell Res.* **32**, 513–529 (2022).
23. M. Yang, H. Yu, X. Yu, S. Liang, Y. Hu, Y. Luo, Z. Izsvák, C. Sun, J. Wang, Chemical-induced chromatin remodeling reprograms mouse ESCs to totipotent-like stem cells. *Cell Stem Cell* **29**, 400–418 (2022).
24. E. R. Barry, W. Krueger, C. M. Jakuba, E. Veilleux, D. J. Ambrosi, C. E. Nelson, T. P. Rasmussen, ES cell cycle progression and differentiation require the action of the histone methyltransferase Dot1L. *Stem Cells* **27**, 1538–1547 (2009).
25. Y. Feng, Y. Yang, M. M. Ortega, J. N. Copeland, M. Zhang, J. B. Jacob, T. A. Fields, J. L. Vivian, P. E. Fields, Early mammalian erythropoiesis requires the Dot1L methyltransferase. *Blood* **116**, 4483–4491 (2010).
26. J. Liao, P. E. Szabó, Maternal DOT1L is dispensable for mouse development. *Sci. Rep.* **10**, 20636 (2020).
27. T. T. Onder, N. Kara, A. Cherry, A. U. Sinha, N. Zhu, K. M. Bernt, P. Cahan, B. O. Marcarci, J. Unternaehrer, P. B. Gupta, E. S. Lander, S. A. Armstrong, G. Q. Daley, Chromatin modifying enzymes as modulators of reprogramming. *Nature* **483**, 598–602 (2012).
28. C. K. Wille, R. Sridharan, DOT1L inhibition enhances pluripotency beyond acquisition of epithelial identity and without immediate suppression of the somatic transcriptome. *Stem Cell Rep.* **17**, 384–396 (2022).
29. C. K. Wille, R. Sridharan, Connecting the DOTs on cell identity. *Front. Cell Dev. Biol.* **10**, 906713 (2022).
30. M. Ooga, M. G. Suzuki, F. Aoki, Involvement of DOT1L in the remodeling of heterochromatin configuration during early preimplantation development in mice. *Biol. Reprod.* **89**, 145 (2013).
31. D. A. Orlando, M. W. Chen, V. E. Brown, S. Solanki, Y. J. Choi, E. R. Olson, C. C. Fritz, J. E. Bradner, M. G. Guenther, Quantitative ChIP-Seq normalization reveals global modulation of the epigenome. *Cell Rep.* **9**, 1163–1170 (2014).
32. F. Frederiks, M. Tzouros, G. Oudgenoeg, T. van Welsem, M. Fornerod, J. Krijgsveld, F. van Leeuwen, Nonprocessive methylation by Dot1 leads to functional redundancy of histone H3K79 methylation states. *Nat. Struct. Mol. Biol.* **15**, 550–557 (2008).
33. M. Sun, B. Schwalb, D. Schulz, N. Pirkl, S. Etzold, L. Larivière, K. C. Maier, M. Seizl, A. Tresch, P. Cramer, Comparative dynamic transcriptome analysis (cDTA) reveals mutual feedback between mRNA synthesis and degradation. *Genome Res.* **22**, 1350–1359 (2012).
34. P. Cramer, Organization and regulation of gene transcription. *Nature* **573**, 45–54 (2019).
35. F. X. Chen, E. R. Smith, A. Shilatifard, Born to run: Control of transcription elongation by RNA polymerase II. *Nat. Rev. Mol. Cell Biol.* **19**, 464–478 (2018).
36. I. Jonkers, J. T. Lis, Getting up to speed with transcription elongation by RNA polymerase II. *Nat. Rev. Mol. Cell Biol.* **16**, 167–177 (2015).
37. L. Core, K. Adelman, Promoter-proximal pausing of RNA polymerase II: A nexus of gene regulation. *Genes Dev.* **33**, 960–982 (2019).
38. B. Gaertner, J. Zeitlinger, RNA polymerase II pausing during development. *Development* **141**, 1179–1183 (2014).
39. D. J. Steger, M. I. Lefterova, L. Ying, A. J. Stonestrom, M. Schupp, D. Zhuo, A. L. Vakoc, J.-E. Kim, J. Chen, M. A. Lazar, G. A. Blobel, C. R. Vakoc, DOT1L/KMT4 recruitment and H3K79 methylation are ubiquitously coupled with gene transcription in mammalian cells. *Mol. Cell. Biol.* **28**, 2825–2839 (2008).
40. P. B. Rahl, C. Y. Lin, A. C. Seila, R. A. Flynn, S. McCuine, C. B. Burge, P. A. Sharp, R. A. Young, c-Myc regulates transcriptional pause release. *Cell* **141**, 432–445 (2010).
41. W. W. M. P. Pijnappel, D. Esch, M. P. A. Baltissen, G. Wu, N. Mischerikow, A. J. Bergsma, E. van der Wal, D. W. Han, H. vom Bruch, S. Moritz, P. Lijnzaad, A. F. M. Altelaar, K. Sameith, H. Zaehres, A. J. R. Heck, F. C. P. Holstege, H. R. Schöler, H. T. M. Timmers, A central role for TFIID in the pluripotent transcription circuitry. *Nature* **495**, 516–519 (2013).
42. M. Kinoshita, M. Barber, W. Mansfield, Y. Cui, D. Spindlow, G. G. Stirparo, S. Dietmann, J. Nichols, A. Smith, Capture of mouse and human stem cells with features of formative pluripotency. *Cell Stem Cell* **28**, 453–471.e8 (2021).
43. R. Shao, B. Kumar, K. Lidschreiber, M. Lidschreiber, P. Cramer, S. J. Elsässer, Distinct transcription kinetics of pluripotent cell states. *Mol. Syst. Biol.* **18**, e10407 (2022).
44. W. Yu, E. J. Chory, A. K. Wernimont, W. Tempel, A. Scopton, A. Federation, J. J. Marineau, J. Qi, D. Barsyte-Lovejoy, J. Yi, R. Marcellus, R. E. Iacob, J. R. Engen, C. Griffin, A. Aman, E. Wienholds, F. Li, J. Pineda, G. Estiu, T. Shatseva, T. Hajian, R. Al-Awar, J. E. Dick, M. Vedadi, P. J. Brown, C. H. Arrowsmith, J. E. Bradner, M. Schapira, Catalytic site remodelling of the DOT1L methyltransferase by selective inhibitors. *Nat. Commun.* **3**, 1288 (2012).
45. G. Nassa, A. Salvati, R. Tarallo, V. Gigantino, E. Alexandrova, D. Memoli, A. Sellitto, F. Rizzo, D. Malanga, T. Mirante, E. Morelli, M. Nees, M. Åkerfelt, S. Kangaspeska, T. A. Nyman, L. Milanesi, G. Giurato, A. Weisz, Inhibition of histone methyltransferase DOT1L silences ERα gene and blocks proliferation of antiestrogen-resistant breast cancer cells. *Sci. Adv.* **5**, eaav5590 (2019).
46. S. A. Jackson, Z. P. G. Olufs, K. A. Tran, N. Z. Zaidan, R. Sridharan, Alternative routes to induced pluripotent stem cells revealed by reprogramming of the neural lineage. *Stem Cell Rep.* **6**, 302–311 (2016).
47. S. Biglione, S. A. Byers, J. P. Price, V. T. Nguyen, O. Bensaude, D. H. Price, W. Maury, Inhibition of HIV-1 replication by P-TEFb inhibitors DRB, seliciclib and flavopiridol correlates with release of free P-TEFb from the large, inactive form of the complex. *Retrovirology* **4**, 47 (2007).
48. A. J. Deshpande, A. Deshpande, A. U. Sinha, L. Chen, J. Chang, A. Cihan, M. Fazio, C.-W. Chen, N. Zhu, R. Koche, L. Dzhekieva, G. Ibáñez, S. Dias, D. Banka, A. Krivtsov, M. Luo, R. G. Roeder, J. E. Bradner, K. M. Bernt, S. A. Armstrong, AF10 regulates progressive H3K79 methylation and HOX gene expression in diverse AML subtypes. *Cancer Cell* **26**, 896–908 (2014).
49. S. Melcer, H. Hezroni, E. Rand, M. Nissim-Rafinia, A. Skoultchi, C. L. Stewart, M. Bustin, E. Meshorer, Histone modifications and lamin A regulate chromatin protein dynamics in early embryonic stem cell differentiation. *Nat. Commun.* **3**, 910 (2012).
50. C. L. Hirsch, Z. Coban Akdemir, L. Wang, G. Jayakumaran, D. Trcka, A. Weiss, J. J. Hernandez, Q. Pan, H. Han, X. Xu, Z. Xia, A. P. Salinger, M. Wilson, F. Vizeacoumar, A. Datti, W. Li, A. J. Cooney, M. C. Barton, B. J. Blencowe, J. L. Wrana, S. Y. R. Dent, Myc and SAGA rewire an alternative splicing network during early somatic cell reprogramming. *Genes Dev.* **29**, 803–816 (2015).
51. L. MacPherson, J. Anokye, M. M. Yeung, E. Y. N. Lam, Y.-C. Chan, C.-F. Weng, P. Yeh, K. Knezevic, M. S. Butler, A. Hoegl, K.-L. Chan, M. L. Burr, L. J. Gearing, T. Willson, J. Liu, J. Choi, Y. Yang, R. A. Bilardi, H. Falk, N. Nguyen, P. A. Stupple, T. S. Peat, M. Zhang, M. de Silva, C. Carrasco-Pozo, V. M. Avery, P. S. Khoo, O. Dolezal, M. L. Dennis, S. Nuttall, R. Surjadi, J. Newman, B. Ren, D. J. Leaver, Y. Sun, J. B. Baell, O. Dovey, G. S. Vassiliou, F. Grebien, S.-J. Dawson, I. P. Street, B. J. Monahan, C. J. Burns, C. Choudhary, M. E. Blewitt, A. K. Voss, T. Thomas, M. A. Dawson, HBO1 is required for the maintenance of leukaemia stem cells. *Nature* **577**, 266–270 (2020).
52. L. A. Gates, J. Shi, A. D. Rohira, Q. Feng, B. Zhu, M. T. Bedford, C. A. Sagum, S. Y. Jung, J. Qin, M.-J. Tsai, S. Y. Tsai, W. Li, C. E. Foulds, B. W. O'Malley, Acetylation on histone H3 lysine 9 mediates a switch from transcription initiation to elongation. *J. Biol. Chem.* **292**, 14456–14472 (2017).
53. C. Lin, E. R. Smith, H. Takahashi, K.-C. Lai, S. Martin-Brown, L. Florens, M. P. Washburn, J. W. Conaway, R. C. Conaway, A. Shilatifard, AFF4, a component of the ELL/P-TEFb elongation complex and a shared subunit of MLL chimeras, can link transcription elongation to leukemia. *Mol. Cell* **37**, 429–437 (2010).
54. Y. Li, B. R. Sabari, T. Panchenko, H. Wen, D. Zhao, H. Guan, L. Wan, H. Huang, Z. Tang, Y. Zhao, R. G. Roeder, X. Shi, C. D. Allis, H. Li, Molecular coupling of histone crotonylation and active transcription by AF9 YEATS domain. *Mol. Cell* **62**, 181–193 (2016).
55. Y. Li, H. Wen, Y. Xi, K. Tanaka, H. Wang, D. Peng, Y. Ren, Q. Jin, S. Y. R. Dent, W. Li, H. Li, X. Shi, AF9 YEATS domain links histone acetylation to DOT1L-mediated H3K79 methylation. *Cell* **159**, 558–571 (2014).
56. S.-K. Kim, I. Jung, H. Lee, K. Kang, M. Kim, K. Jeong, C. S. Kwon, Y.-M. Han, Y. S. Kim, D. Kim, D. Lee, Human histone H3K79 methyltransferase DOT1L methyltransferase binds actively transcribing RNA polymerase II to regulate gene expression. *J. Biol. Chem.* **287**, 39698–39709 (2012).
57. A. Bulut-Karslioglu, T. A. Macrae, J. A. Oses-Prieto, S. Covarrubias, M. Percharde, G. Ku, A. Diaz, M. T. McManus, A. L. Burlingame, M. Ramalho-Santos, The transcriptionally permissive chromatin state of embryonic stem cells is acutely tuned to translational output. *Cell Stem Cell* **22**, 369–383.e8 (2018).
58. L. H. Williams, G. Fromm, N. G. Gokey, T. Henriques, G. W. Muse, A. Burkholder, D. C. Fargo, G. Hu, K. Adelman, Pausing of RNA polymerase II regulates mammalian developmental potential through control of signaling networks. *Mol. Cell* **58**, 311–322 (2015).
59. A. Strikoudis, C. Lazaris, T. Trimarchi, A. L. Galvao Neto, Y. Yang, P. Ntziachristos, S. Rothbart, S. Buckley, I. Dolgalev, M. Stadtfeld, B. D. Strahl, B. D. Dynlacht, A. Tsirigos, I. Aifantis, Regulation of transcriptional elongation in pluripotency and cell differentiation by the PHD-finger protein Phf5a. *Nat. Cell Biol.* **18**, 1127–1138 (2016).
60. J. Bonnet, C.-Y. Wang, T. Baptista, S. D. Vincent, W.-C. Hsiao, M. Stierle, C.-F. Kao, L. Tora, D. Devys, The SAGA coactivator complex acts on the whole transcribed genome and is required for RNA polymerase II transcription. *Genes Dev.* **28**, 1999–2012 (2014).
61. A. Wu, J. Zhi, T. Tian, A. Cihan, M. A. Cevher, Z. Liu, Y. David, T. W. Muir, R. G. Roeder, M. Yu, DOT1L complex regulates transcriptional initiation in human erythroleukemic cells. *Proc. Natl. Acad. Sci. U.S.A.* **118**, e2106148118 (2021).
62. G. Cecere, S. Hoersch, M. B. Jensen, S. Dixit, A. Grishok, The ZFP-1(AF10)/DOT-1 complex opposes H2B ubiquitination to reduce Pol II transcription. *Mol. Cell* **50**, 894–907 (2013).
63. K.-P. Kim, J. Choi, J. Yoon, J. M. Bruder, B. Shin, J. Kim, M. J. Arauzo-Bravo, D. Han, G. Wu, D. W. Han, J. Kim, P. Cramer, H. R. Schöler, Permissive epigenomes endow reprogramming competence to transcriptional regulators. *Nat. Chem. Biol.* **17**, 47–56 (2021).

64. V. Oksenych, A. Zhovmer, S. Ziani, P.-O. Mari, J. Eberova, T. Nardo, M. Stefanini, G. Giglia-Mari, J.-M. Egly, F. Coin, Histone methyltransferase DOT1L drives recovery of gene expression after a genotoxic attack. *PLOS Genet.* **9**, e1003611 (2013).
65. M. A. Aslam, M. F. Alemdehy, E. M. Kwesi-Maliepaard, F. I. Muhaimin, M. Caganova, I. N. Pardieck, T. van den Brand, T. van Welsem, I. de Rink, J.-Y. Song, E. de Wit, R. Arens, H. Jacobs, F. van Leeuwen, Histone methyltransferase DOT1L controls state-specific identity during B cell differentiation. *EMBO Rep.* **22**, e51184 (2021).
66. F. Ferrari, L. Arrigoni, H. Franz, A. Izzo, L. Butenko, E. Trompouki, T. Vogel, T. Manke, DOT1L-mediated murine neuronal differentiation associates with H3K79me2 accumulation and preserves SOX2-enhancer accessibility. *Nat. Commun.* **11**, 5200 (2020).
67. L. Godfrey, N. T. Crump, R. Thorne, I.-J. Lau, E. Repapi, D. Dimou, A. L. Smith, J. R. Harman, J. M. Telenius, A. M. Oudelaar, D. J. Downes, P. Vyas, J. R. Hughes, T. A. Milne, DOT1L inhibition reveals a distinct subset of enhancers dependent on H3K79 methylation. *Nat. Commun.* **10**, 2803 (2019).
68. E. M. Kwesi-Maliepaard, M. A. Aslam, M. F. Alemdehy, T. van den Brand, C. McLean, H. Vlaming, T. van Welsem, T. Korthout, C. Lancini, S. Hendriks, T. Ahrends, D. van Dinther, J. M. M. den Haan, J. Borst, E. de Wit, F. van Leeuwen, H. Jacobs, The histone methyltransferase DOT1L prevents antigen-independent differentiation and safeguards epigenetic identity of CD8+ T cells. *Proc. Natl. Acad. Sci. U.S.A.* **117**, 20706–20716 (2020).
69. W. F. Richter, R. N. Shah, A. J. Ruthenburg, Non-canonical H3K79me2-dependent pathways promote the survival of MLL-rearranged leukemia. *eLife* **10**, e64960 (2021).
70. K. A. Tran, S. J. Pietrzak, N. Z. Zaidan, A. F. Siahpirani, S. G. McCalla, A. S. Zhou, G. Iyer, S. Roy, R. Sridharan, Defining reprogramming checkpoints from single-cell analyses of induced pluripotency. *Cell Rep.* **27**, 1726–1741.e5 (2019).
71. C. Beard, K. Hochedlinger, K. Plath, A. Wutz, R. Jaenisch, Efficient method to generate single-copy transgenic mice by site-specific integration in embryonic stem cells. *Genesis* **44**, 23–28 (2006).
72. H. Marks, T. Kalkan, R. Menafra, S. Denissov, K. Jones, H. Hofemeister, J. Nichols, A. Kranz, A. F. Stewart, A. Smith, H. G. Stunnenberg, The transcriptional and epigenomic foundations of ground state pluripotency. *Cell* **149**, 590–604 (2012).
73. S. P. Thomas, S. A. Haws, L. E. Borth, J. M. Denu, A practical guide for analysis of histone post-translational modifications by mass spectrometry: Best practices and pitfalls. *Methods* **184**, 53–60 (2020).
74. Z.-F. Yuan, S. Sidoli, D. M. Marchione, J. Simithy, K. A. Janssen, M. R. Szurgot, B. A. Garcia, EpiProfile 2.0: A computational platform for processing epi-proteomics mass spectrometry data. *J. Proteome Res.* **17**, 2533–2541 (2018).
75. B. Langmead, S. L. Salzberg, Fast gapped-read alignment with Bowtie 2. *Nat. Methods* **9**, 357–359 (2012).
76. H. Li, B. Handsaker, A. Wysoker, T. Fennell, J. Ruan, N. Homer, G. Marth, G. Abecasis, R. Durbin; 1000 Genome Project Data Processing Subgroup, The Sequence Alignment/Map format and SAMtools. *Bioinformatics* **25**, 2078–2079 (2009).
77. Y. Zhang, T. Liu, C. A. Meyer, J. Eeckhoute, D. S. Johnson, B. E. Bernstein, C. Nusbaum, R. M. Myers, M. Brown, W. Li, X. S. Liu, Model-based analysis of ChIP-Seq (MACS). *Genome Biol.* **9**, R137 (2008).
78. J. T. Robinson, H. Thorvaldsdóttir, W. Winckler, M. Guttman, E. S. Lander, G. Getz, J. P. Mesirov, Integrative genomics viewer. *Nat. Biotechnol.* **29**, 24–26 (2011).
79. S. Heinz, C. Benner, N. Spann, E. Bertolino, Y. C. Lin, P. Laslo, J. X. Cheng, C. Murre, H. Singh, C. K. Glass, Simple combinations of lineage-determining transcription factors prime cis-regulatory elements required for macrophage and B cell identities. *Mol. Cell* **38**, 576–589 (2010).
80. F. Ramírez, D. P. Ryan, B. Grüning, V. Bhardwaj, F. Kilpert, A. S. Richter, S. Heyne, F. Dündar, T. Manke, deepTools2: A next generation web server for deep-sequencing data analysis. *Nucleic Acids Res.* **44**, W160–W165 (2016).
81. A. R. Quinlan, I. M. Hall, BEDTools: A flexible suite of utilities for comparing genomic features. *Bioinformatics* **26**, 841–842 (2010).
82. B. Kalveram, O. Lihoradova, S. V. Indran, J. A. Head, T. Ikegami, Using click chemistry to measure the effect of viral infection on host-cell RNA synthesis. *J. Vis. Exp.* **9**, 50809 (2013).
83. I. Jonkers, H. Kwak, J. T. Lis, Genome-wide dynamics of Pol II elongation and its interplay with promoter proximal pausing, chromatin, and exons. *eLife* **3**, e02407 (2014).
84. C. M. Nefzger, F. J. Rossello, J. Chen, X. Liu, A. S. Knaupp, J. Firas, J. M. Paynter, J. Pflueger, S. Buckberry, S. M. Lim, B. Williams, S. Alaei, K. Faye-Chauhan, E. Petretto, S. K. Nilsson, R. Lister, M. Ramialison, D. R. Powell, O. J. L. Rackham, J. M. Polo, Cell type of origin dictates the route to pluripotency. *Cell Rep.* **21**, 2649–2660 (2017).
85. H. Franz, A. Villarreal, S. Heidrich, P. Videm, F. Kilpert, I. Mestres, F. Calegari, R. Backofen, T. Manke, T. Vogel, DOT1L promotes progenitor proliferation and primes neuronal layer identity in the developing cerebral cortex. *Nucleic Acids Res.* **47**, 168–183 (2019).

Acknowledgments: We thank R. Wille for aid in statistical analysis and script design, A. Tak for quantifying microscopy images, S. Pietrzak for experimental support, and members of the Sridharan laboratory for critical reading of the manuscript. **Funding:** This work was supported by NIH-NIGMS 2R01GM113033, UW-Madison PARCI Award, and Shaw Scientist Award to R.S. and R35GM149279 to J.M.D. **Author contributions:** Conceptualization: R.S., C.K.W., and X.Z. Methodology: C.K.W., R.S., and X.Z. Investigation: C.K.W., X.Z., and S.A.H. Validation: C.K.W. and R.S. Visualization: C.K.W. Supervision: R.S. Funding acquisition: R.S. Resources: J.M.D. Writing—original draft: C.K.W. and R.S. Writing—review and editing: C.K.W., R.S., J.M.D., and X.Z. **Competing interests:** J.M.D. is cofounder of Galilei Bioscience and a consultant for Evrys Bio. All other authors declare that they have no competing interests. **Data and materials availability:** All data needed to evaluate the conclusions in the paper are present in the paper and/or the Supplementary Materials. All ChIP-seq datasets have been submitted to the National Center for Biotechnology Information Gene Expression Omnibus database GSE190391.

Submitted 18 October 2022
Accepted 18 October 2023
Published 17 November 2023
10.1126/sciadv.adf3980